THESIS

SUPERHYDROPHOBIC TITANIA NANOFLOWERS FOR REDUCING ADHESION OF PLATELETS AND BACTERIA

Submitted by

Zachary Z. Montgomerie

Department of Mechanical Engineering

In partial fulfillment of the requirements

For the Degree of Master of Science

Colorado State University

Fort Collins, Colorado

Summer 2020

Master's Committee:

Advisor: Ketul C. Popat

Vivian Li
Walajabad S. Sampath

ABSTRACT

SUPERHYDROPHOBIC TITANIA NANOFLOWERS FOR REDUCING ADHESION OF PLATELETS AND BACTERIA

Thrombosis formation and bacterial infection are key challenges for blood-contacting medical devices. When blood components encounter a device's surface, proteins are adsorbed, followed by the adhesion and activation of platelets as well as an immune response. This culminates in clot formation via the trapping of red blood cells in a fibrin matrix, which can block the device's function and cause severe complications for the patient. Bacteria may also adhere to a device's surface. This can lead to the formation of a biofilm, a protective layer for bacteria that significantly increases resistance to antibiotics. Despite years of research, no long-term solutions have been discovered to combat these issues. To impede thrombosis, patients often take antiplatelet drugs for the life of their device, which can cause excess bleeding and other complications. Patients can take antibiotics to fight bacterial infection, but these are often ineffective if biofilms are formed. Superhydrophobic surfaces have recently been studied for their antiadhesive properties and show promise in reducing both thrombosis and bacterial infection. In this work, superhydrophobic titania nanoflower surfaces were successfully fabricated on a titanium alloy Ti-6Al-4V substrate and examined for both hemocompatibility and bacterial adhesion. The results indicated a reduction of protein adsorption, platelet and leukocyte adhesion and activation, whole blood clotting, bacterial adhesion, and biofilm formation, as well as surface stability compared to control surfaces.

ACKNOWLEDGEMENTS

First and foremost, I would like to thank my advisor, Dr. Ketul Popat, for his guidance from the beginning of my junior year up until now. I could not have asked for a more patient, caring, and intelligent mentor throughout my graduate work. Thank you.

I would like to thank Dr. Patrick McCurdy from the chemistry department for teaching me how to operate a scanning electron microscope and an X-ray spectroscopy machine. These are two valuable skills I am sure will come in handy later in my career.

I would also like to thank Dr. Paolo Soares of Pontifical Catholic University of Paraná in Curitiba, Brazil for his help in analyzing material samples for X-ray diffraction.

Finally, I would like to especially thank my colleagues in the lab: Robert Sabino, Vignesh Manivasagam, Sayudh Ghosh, and Prem Kantam. Roberta has always been so kind and helpful over the past two years. She has taught me almost every laboratory technique I know and has answered countless questions of mine. Vignesh and I started in the lab around the same time and it has been a pleasure working alongside him. He taught me how to carry out bacteria studies and has always been there to help when I needed it. Sayudh and Prem were always wonderful to be around and both have incredible work ethic. I wish you all the best in your future endeavors and I cannot wait to see what marvelous things you will accomplish.

DEDICATION

I would like to dedicate this thesis to my late grandmother, Claudia Anderson, who sadly passed away in May of this year. She was so strong and sacrificed so much so I could live the life I live. I love you.

TABLE OF CONTENTS

ABSTRACT ii

ACKNOWLEDGEMENTS iii

DEDICATION iv

LIST OF FIGURES vii

INTRODUCTION 1

HYPOTHESIS AND SPECIFIC AIMS 4

CHAPTER 1 5
LITERATURE REVIEW 5
1.1 Introduction 5
1.2 Thrombus formation on surfaces 6
1.3 Blood-contacting devices 8
1.4 Bacterial Infection on surfaces 11
1.5 Current solutions for thrombosis and bacterial infections on biomedical devices 14
1.6 Superhydrophobic materials 17
1.7 Titanium and titania nanomodification in biomaterials 21
REFERENCES 24

CHAPTER 2 33
FABRICATION AND CHARACTERIZATION OF TITANIA NANOFLOWER SURFACES 33
2.1 Introduction 33
2.2 Materials and Methods 33
2.3 Results and Discussion 36
REFERENCES 46

CHAPTER 3 48
HEMOCOMPATIBILITY OF TITANIA NANOFLOWER SURFACES 48
3.1 Introduction 48
3.2 Materials and Methods 48

3.3 Results and Discussion 52
REFERENCES 63

CHAPTER 4 64
BACTERIAL ADHESION ON TITANIA NANOFLOWERS 64
4.1 Introduction 64
4.2 Materials and Methods 64
4.3 Results and Discussion 66
REFERENCES 75

CHAPTER 5 76
CONCLUSIONS AND FUTURE WORK 76
5.1 Conclusions 76
5.2 Future Work 78

LIST OF FIGURES

Figure 1.2.1: Graphical representation of thrombosis on medical device surfaces. Protein adsorption leads to platelet adhesion, activation, and aggregation. FXII absorbs and auto activates, converting prekallikrein to kallikrein while initiating coagulation and thrombin generation. Thrombin promotes platelet activation, and converts fibrinogen into fibrin. Polymerized fibrin stabilizes platelet aggregates, forming a thrombus. Kallikrein, thrombin and other coagulation enzymes activate complement, inducing a local inflammatory response. Leukocytes are adhered, activated, and contribute to both coagulation and inflammation. Adapted with permission from Elsevier Ltd: [Acta Biomaterialia Vol. 94] I.H. Jaffer, J.I. Weitz, The blood compatibility challenge. Part 1: Blood-contacting medical devices: The scope of the problem. Copyright (2019). License at https://creativecommons.org/licenses/by-nc-nd/4.0/ [16] 8

Figure 1.3.1: Examples of blood-contacting devices: (A) coronary stent, (B) mechanical heart valve, and (C) a left ventricular assist device. (A) adapted with permission from Blausen.com staff (2014). "Medical gallery of Blausen Medical 2014". WikiJournal of Medicine. (B) and (C) adapted from the National Library of Medicine and the National Heart Lung and Blood Institute, respectively 11

Figure 1.4.1: The processes of biofilm formation on device surfaces. Adapted with permission from the American Society for Microbiology: [ASM News Vol. 70 N. 5] J. Bryers, Ratner BD, Bioinspired implant materials befuddle bacteria. Copyright (2004). License at https://creativecommons.org/licenses/by-nc-sa/3.0/ [53]. 14

Figure 1.6.1: Depiction of (A) Young, (B) Wenzel, and (C) Cassie-Baxter wetting models. Adapted with permission from Elsevier B.V.: [Arabian Journal of Chemistry Vol. 13 Iss. 1] G. Barati Darband, M. Aliofkhazraei, S. Khorsand, S. Sokhanvar, A. Kaboli, Science and Engineering of Superhydrophobic Surfaces: Review of Corrosion Resistance, Chemical and Mechanical Stability. Copyright (2018). License at https://creativecommons.org/licenses/by-nc-nd/4.0/ [85]..... 18

Figure 1.6.2: Example depiction of hydrolytic deposition of a trichlorosilane to a substrate 20

Figure 1.7.1: Examples of titania (A) nanoleaves, (B), nanotubes, and (C) nanoflowers. (B) and (C). (A) adapted with permission from John Wiley and Sons: [Advanced Healthcare Materials Vol. 6 Iss. 11] C.C. Mohan, A.M. Cherian, S. Kurup, J. Joseph, M.B. Nair, M. Vijayakumar, S. V. Nair, D. Menon, Stable Titania Nanostructures on Stainless Steel Coronary Stent Surface for Enhanced Corrosion Resistance and Endothelialization. Copyright (2017). [119]. (B) adapted with permission from The Royal Society of Chemistry: [RSC Advances Vol. 7] K. Bartlet, S. Movafaghi, A. Kota, K.C. Popat, Superhemophobic titania nanotube array surfaces for blood contacting medical devices. Copyright (2017). License at https://creativecommons.org/licenses/by-nc-sa/3.0/ [101] 23

Figure 2.3.1: Representative SEM images of control and titania nanoflower surfaces fabricated using hydrothermal synthesis and vapor-phase silanization 38

Figure 2.3.2: XPS survey scans for Ti, Ti-s, NF, and NF-s surfaces 40

Figure 2.3.3: XRD scans of Ti, Ti-s, NF, and NF-s surfaces 41

Figure 2.3.4: Contact angle measurements on Ti, Ti-s, NF, and NF-s surfaces incubated in air (A) and PBS (B) over a 4-week period. A slight decrease was seen in contact angle for NF-s in PBS ($p \leq 0.05$). Note: statistics are discussed further in results and discussion..... 43

Figure 2.3.5: High resolution C1s XPS scans of as-fabricated surfaces and surfaces incubated in air and PBS for 4 weeks 45

Figure 3.3.1: Cytotoxicity results from a commercially available LDH assay. All surfaces showed minimal cytotoxicity compared to the positive control ($p \leq 0.05$) 52

Figure 3.3.2: High resolution N1s XPS scans indicate the presence of protein on the surfaces 54

Figure 3.3.3: (A) Representative fluorescence microscopy images of calcein-AM-stained cells on different surfaces. (B) Cell surface adhesion area as a percentage on different surfaces (calcein-AM stain). NF-s showed significantly lower cell adhesion ($p \leq 0.05$) 57

Figure 3.3.4: (A) Representative fluorescence microscopy images of rhodamine-phalloidin and DAPI stained cells on different surfaces. (B) Cell surface adhesion area as a percentage on different surfaces (rhodamine-phalloidin stain) and (C) Leukocytes per mm^2 (DAPI stain). NF-s showed significantly lower cell and leukocyte adhesion ($p \leq 0.05$) 59

Figure 3.3.5: (A) Representative SEM images of cell activation on various surfaces. (B) Platelet count on different surfaces. NF-s was shown to have the lowest number of fully activated platelets ($p \leq 0.05$). 61

Figure 3.3.6: Whole blood clotting indicated by free hemoglobin absorbance measured after 15, 30, and 45 mins. Note: statistics are discussed in results and discussion 62

Figure 4.3.1: (A) Representative fluorescence images of *S. aureus* on different surfaces. Bacterial cell adhesion area percentage for live (B) and dead (C) *S. aureus* after 6 and 24 hrs. Note: statistics discussed in results and discussion 69

Figure 4.3.2: (A) Representative fluorescence images of *E. coli* on different surfaces. Bacterial cell adhesion area percentage for live (B) and dead (C) *E. coli* after 6 and 24 hrs. Note: statistics discussed in results and discussion..... 71

Figure 4.3.3: Representative SEM images of *S. aureus* (A) and *E. coli* (B) on different surfaces 74

INTRODUCTION

Blood-contacting medical devices, such as stents and heart valves, are common treatments in modern healthcare. However, thrombosis and bacterial infection can complicate the use of these devices. Thrombosis is the process of blood clot formation and begins with the immediate deposition of blood-plasma proteins, mainly fibrinogen, on a device surface. Meanwhile, factor XII, another plasma protein, is deposited and facilitates thrombin formation via several reactions. The thrombin reacts with fibrinogen to form fibrin which helps bind blood cells and activated platelets to form a clot. These clots can impede a device's function, cause severe injury, or even death. Despite many years of research, a completely antithrombic surface has yet to be created. In addition, the threat of bacterial infection on these devices is a significant concern in the short and long-term. Bacterial adhesion on a device surface can lead to the formation of a biofilm, a protective layer composed primarily of proteins and polysaccharides that makes treatment with antibiotics difficult. Research also suggests that bacterial infections may lead to overactivation of the coagulation system, worsening thrombosis. For these reasons, the development of biomaterials that can simultaneously reduce thrombosis and bacterial infection is vital.

Many different approaches have been advanced to combat thrombosis and bacterial adhesion on blood-contacting devices. The most common method to protect against thrombosis is to prescribe antiplatelet therapy with blood thinners, such as aspirin, which reduce the tendency for platelets to adhere and activate. However, the drawbacks of these drugs may include drug resistance, excess bleeding, and the need for long-term usage. Another approach is to coat the device surface with heparin, an anticoagulant, which seeks to immobilize thrombin. Challenges faced with heparin coatings include difficulty binding heparin to the antithrombin molecule it acts on, and degradation of heparin due to stresses imposed within the body. More recently, nitric oxide (NO) releasing surfaces have been studied since NO naturally occurs in blood vessels and

has both antithrombotic and antibacterial properties. Although these surfaces have shown promise, the release of NO must be controlled and sustained long-term, which has proven difficult. Methods for reducing bacterial adhesion on surfaces have most often included the use of local or systemically released antibiotics, and silver-releasing coatings. With these methods, antibiotic resistance of biofilms and damage to human cells have been significant concerns, respectively. Thus, no single antibacterial strategy has proven effective long-term.

Titanium and its alloys have been widely used in medical device applications for many years due to its general compatibility with bone tissues and ideal mechanical properties. However, titanium devices are associated with many of the problems mentioned previously, and the material is not generally considered hemocompatible or antibacterial in its unaltered form. Recently, research into the modification of the stable oxide layer (TiO_2) nanotexture formed on titanium surfaces has shown promise in reducing thrombosis and bacterial adhesion. Nanotextures can be created using different fabrication techniques such as anodization, sol-gel, or hydrothermal synthesis. The hydrothermal synthesis technique is especially attractive because of its simplicity, low cost, and the ability to vary parameters to obtain different surface feature roughness, size, or shape. In addition to modifying nanotexture, modification of surface chemistry to create low surface-energy superhydrophobic nanotextured surfaces shows great potential for increasing antiadhesive properties. For example, research has shown superhydrophobic nanotubes reduce protein adsorption and platelet adhesion/activation, key processes that lead to thrombosis, as well as the adhesion of Gram-positive and Gram-negative bacteria. The combination of a nanotexture and low surface-energy creates the Cassie Baxter state, which provides a protective air-film layer and allows a high surface contact angle, severely limiting interaction between blood components/bacteria and the surface.

In this work, superhydrophobic titania nanoflowers were successfully fabricated for the first time on titanium alloy Ti-6Al-4V with the goal of improving hemocompatibility and reducing bacterial adhesion. Platelet adhesion and activation has previously been shown to be reduced on

superhydrophobic titania nanoflowers grown from commercially pure titanium (CpTi) compared to a control CpTi surface. However, interaction between individual blood components and the surface or bacteria and the surface has not been fully characterized, nor the behavior of nanoflowers grown from a Ti-6Al-4V substrate. In this study, an alloy surface was first modified to create titania nanoflowers using hydrothermal synthesis, and then treated using a vapor-phase silanization technique to create a superhydrophobic surface. The material was characterized using scanning electron microscopy (SEM), contact angle goniometry, X-ray photoelectron spectroscopy (XPS), and X-ray diffraction (XRD). The surface cytotoxicity, protein adsorption, platelet/leukocyte adhesion, platelet activation, and whole blood clotting were investigated in addition to the adhesion and morphology of Gram-positive and Gram-negative bacteria. The results indicate improved antithrombic and antibacterial properties on superhydrophobic titania nanoflowers in comparison to control surfaces.

HYPOTHESIS AND SPECIFIC AIMS

Fundamental Hypothesis: Superhydrophobic titania nanoflowers can reduce attachment of blood-plasma proteins, platelets, leukocytes, and bacteria.

Hypothesis 1: Titania nanoflowers can be silanized to create a stable superhydrophobic surface.

Specific Aim 1: Fabrication and characterization of superhydrophobic titania nanoflowers. This specific aim is discussed in chapter 2 and will cover:

(a) Fabrication of uniformly distributed and reproducible titania nanoflower surfaces via hydrothermal synthesis

(b) Fabrication of a superhydrophobic surface coating through modification of surface chemistry

(c) Characterization of titania nanoflower surfaces and measurement of water contact angles

Hypothesis 2: Superhydrophobic titania nanoflowers can improve hemocompatibility and reduce biofilm formation by reducing bacterial adhesion

Specific Aim 2: Characterization of protein adsorption, adhesion and activation of blood components, and bacterial adhesion on titania nanoflowers. This specific aim is discussed in chapters 3 and 4 and will cover:

(a) Investigation of cytotoxicity, blood protein adsorption, platelet and leukocyte adhesion and activation, and whole blood clotting

(b) Adhesion and morphology of Gram-positive and Gram-negative bacteria

Chapter 1

LITERATURE REVIEW

1.1 Introduction

Blood-contacting medical devices, such as stents and heart valves, are common treatments in modern healthcare. However, thrombus formation and bacterial infection may complicate the use of these devices upon implantation. Thrombosis occurs when the body recognizes the artificial material of the device surface as a foreign object. This initiates deposition and activation of blood components, leading to immune response and blood clot formation on the surface. These clots can impede the device's original function and cause severe complications upon detachment. Bacterial infection on blood-contacting devices can be initiated through the device's exposure to bacteria when it is implanted, or from the patient's own microflora. Once bacteria adhere to the device's surface, they may begin to form biofilms. The biofilm supplies bacteria with protection and nourishment, and increases communication between bacteria to significantly increase antibiotic resistance. Bacterial infections left untreated may lead to device failure, sepsis, or even death. Current treatments for blood-contacting devices largely consist of drug therapies to maintain and treat thrombosis and infection. However, these solutions present problems of their own and do not work long-term. Therefore, many researchers are working to modify the device surface itself to increase bio-integration and reduce infection. These methods generally consist of fabrication of a drug or therapeutic surface coating in combination with modification of surface topography, chemistry, or charge. Today, titanium and its alloys are widely used in many types of medical devices as they show favorable mechanical properties. Recent research has focused on the modification of the titanium dioxide (TiO_2) layer formed on titanium surfaces for improving surface hemocompatibility. Nanotextures made from this titania layer indicate improved compatibility with various bone and cardiovascular cells. More recently, superhydrophobic surfaces have been fabricated from titania nanotextures by modifying surface

chemistry. Studies of these surfaces indicate reduced adhesion of blood components and bacteria by limiting interaction between the surface and biological elements. Therefore, superhydrophobic surfaces show promise for reducing thrombosis and bacterial infection; however, more data is needed to verify the potential of these surfaces.

1.2 Thrombus formation on surfaces

Unlike healthy endothelium, which actively resists thrombosis within the arterial lining, implanted artificial surfaces promote thrombosis through a series of complex interconnected processes [1]. Thrombosis begins with the immediate deposition of blood-plasma proteins on a device surface. This is followed by the adhesion and activation of platelets and leukocytes, which leads to thrombus fabricated from these components and red blood cells (RBCs). Of the roughly 300 distinct proteins contained within blood-plasma, fibrinogen is one of the first to adsorb onto the artificial surface and is central to mediating platelet adhesion [1]. Fibrinogen-platelet adhesion is mediated by glycoprotein protein complex IIb-IIIa on platelets and can readily occur even when fibrinogen levels are extremely reduced [2,3]. After adhering to a surface, platelets may be activated by different chemical indicators such as exposed collagen or thrombin [4] or from a negative surface charge [5]. Activated platelets release thromboxane A_2, adenosine diphosphate (ADP), and other agonists which further the adhesion, activation, and aggregation of other platelets [1]. Leukocytes are adhered to deposited fibrinogen via complement receptor type 3 (CD11b/CD18 and CD11c/CD18) of the complement activation system [6,7]. P-selectin on adhered platelets activates P-selectin glycoprotein ligand-1 (PSGL-1), a counter receptor on leukocytes, that leads to activation of beta-2 integrin Mac-1 and stabilized platelet-leukocyte aggregates [8]. The interaction between P-selectin and PSGL-1 also induces upregulation of leukocyte tissue factor, biosynthesis of several cytokines and other inflammatory reactions, thus increasing thrombosis [8].

Blood clot formation occurs as absorbed fibrinogen is gradually replaced via the Vroman effect by proteins of the contact system, including factor (F) XII, high molecular weight kininogen, prekallikrein, and FXI [9]. Autoactivated FXII (FXIIa) initiates thrombin formation as part of the intrinsic pathway of the coagulation cascade and turns PK into kallikrein, which in turn activates more FXII [1,10]. Kallikrein cleaves FXIIa to form β-FXIIa, which triggers the classical pathway of the complement system via activation of the C1q complex protein [10,11]. Kallikrein also activates C3 and C5, two protein complexes of the complement system, while FIXa, FXa, and thrombin of the coagulation cascade activate C5 [10–12]. Activated C3 and C5 further promote the adhesion and activation of leukocytes to artificial surfaces [11]. Resulting cross communication between coagulation and complement systems increases thrombin production and inflammatory response [11]. In addition to converting fibrinogen into fibrin monomers, thrombin also serves as a platelet agonist and furthers platelet aggregation [1]. Fibrin monomers polymerize on the device surface, stabilizing the platelet aggregates that form thrombus [1,10]. Furthermore, activated leukocytes are often observed within thrombi [13]. The role of RBC adhesion to the thrombus has long been considered a passive process, yet recent studies suggest that RBCs use chemical indicators to bind with fibrinogen, thrombin, and platelets [14,15]. However, the exact mechanisms and sequences for this are still under study and research has not been carried out specifically regarding RBCs and artificial-device thrombosis. Nonetheless, the final thrombus is often a complex matrix of proteins, platelets, leukocytes, and RBCs. A visual representation of thrombosis is shown below (**figure 1.2.1**). Thrombi can cause device failure, or detach and travel through various blood vessels, leading to clotting or death. Therefore, it is necessary to develop medical devices that can impede thrombosis, and understanding the mechanisms of thrombus formation is vital to engineering these solutions.

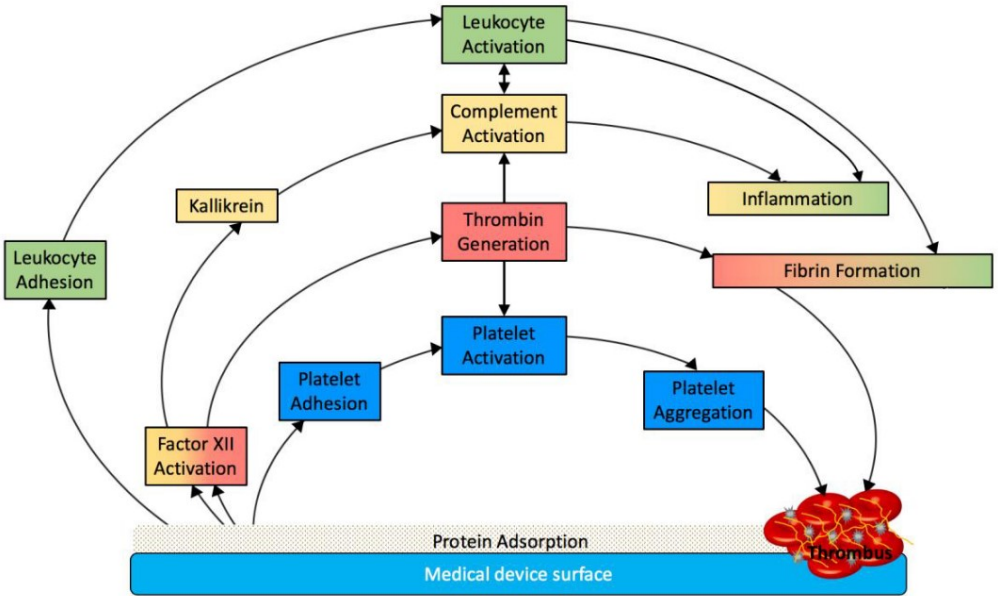

Figure 1.2.1: Graphical representation of thrombosis on medical device surfaces. Protein adsorption leads to platelet adhesion, activation, and aggregation. FXII absorbs and auto activates, converting prekallikrein to kallikrein while initiating coagulation and thrombin generation. Thrombin promotes platelet activation, and converts fibrinogen into fibrin. Polymerized fibrin stabilizes platelet aggregates, forming a thrombus. Kallikrein, thrombin and other coagulation enzymes activate complement, inducing a local inflammatory response. Leukocytes are adhered, activated, and contribute to both coagulation and inflammation. Adapted with permission from Elsevier Ltd: [Acta Biomaterialia Vol. 94] I.H. Jaffer, J.I. Weitz, The blood compatibility challenge. Part 1: Blood-contacting medical devices: The scope of the problem. Copyright (2019). License at https://creativecommons.org/licenses/by-nc-nd/4.0/ [16].

1.3 Blood-contacting devices

Coronary stents are commonly used to treat coronary artery disease (CAD), the leading causes of mortality and morbidity in the world [17]. CAD is most often caused by atherosclerosis, the combination of inflammation and build-up of fatty plaque deposits that leads to the narrowing of arteries [18–20]. Interventions to re-expand narrowed arteries began with balloon angioplasty, where a balloon is inserted into the artery and inflated against the arterial lining to remove blockages [21]. Unfortunately, this method often causes elastic recoil and restenosis (re-narrowing of the artery) among other complications [17,21]. This led to the development of coronary stents, which sought to improve these issues. Today, stents are used in roughly 90% of percutaneous coronary intervention procedures [22] as they generally improve long-term patient

outcomes. The first generation of stents were constructed with metal alloys and were deemed bare-metal stents (BMS). Metals used as BMS include: stainless steel, cobalt, and nickel-titanium (nitinol) [23,24]. The high mechanical strength of BMS are ideal for maintaining arterial diameter; however, they are often associated with restenosis caused by scar-tissue formation as well as thrombosis [25]. To combat these complications, drug-eluting stents (DES) were developed and became the standard for stenting. DES contain drugs such as sirolimus and paclitaxel that release to the surrounding endothelium, and usually act to impede vascular smooth muscle cell proliferation that contributes to stent restenosis [25]. DES greatly decrease restenosis; however, DES have not been shown to reduce thrombosis in comparison to BMS [25,26] and thrombosis can occur suddenly late after implantation. Thus, dual antiplatelet therapy (DAPT) with aspirin and clopidogrel, ticagrelor, or prasugrel is usually recommended for at least 6 to 12 months after stent implantation to reduce thrombus formation [10]. However, DAPT can cause excessive bleeding and some patients may become resistant to aspirin [27]. Therefore, stenting solutions that decrease both restenosis and thrombosis without these drawbacks remain a necessity.

Artificial heart valves are another common cardiac device and are used to treat heart valve disease. In 2014 there were 110,915 surgical heart valve procedures performed in the united states, many of which involved the implantation of artificial heart valves [28]. Heart valves can be inserted surgically or through a transcatheter procedure. Mechanical heart valves (MHVs) are generally more thrombogenic than biosynthetic heart valves (BHVs), which are constructed from bovine or porcine tissue mounted on a metal frame [29]. However, BHVs generally need replacement after 10 to 20 years whereas MHVs can last a patient's lifetime [30]. In addition to the promotion of thrombosis through the intrinsic coagulation pathway, hemodynamic and hemostatic factors can increase thrombosis on heart valves. Hemodynamic factors largely include turbulent flows that can damage tissue around the prosthesis, induce platelet adhesion, and prevent repair of the damaged endothelial cell lining (reendothelialization) [29]. Lower fluid flows found near tricuspid and mitral valve protheses also appear to increase thrombosis in comparison

to aortic valve protheses [29]. This may be due to the congregation of coagulation factors near the valve. Hemostatic factors include hypercoagulability caused by diseases like chronic kidney disease, smoking, and obesity [29]. Another factor is tissue damage caused by surgical insertion that activates tissue factor and therefore the extrinsic pathway of coagulation [29,31]. To prevent thrombosis, patients with MHVs are almost always prescribed blood-thinning medications for the rest of their lives [30].

Further blood-contacting medical devices include left ventricular assist devices (LVADs) and extra-corporeal circuits. LVADs are medical devices that pump blood from the lower chambers of the heart to the rest of the patient's body. Although LVADs are rarely used, their maintenance is expensive and patients often experience pump thrombosis, or clotting within the device [10]. In addition, the occurrence of thrombosis in the heartmate II, a commonly used LVAD, appears to be rising according to a study of patients who received the device between 2004 and 2013 [32]. Extra-corporeal circuits are used to replace the function of the heart and lungs during cardiac surgery or when a patient is unable to perform these functions due to organ failure, a process called extracorporeal membrane oxygenation (ECMO). In these circuits, blood is in contact with tubing that promotes thrombosis. Thus, patients are prescribed anticoagulants like heparin, which may increase the risk of bleeding. A study of ECMO patients found bleeding and thrombosis occurred in 38% and 31% of patients, respectively, increasing mortality and morbidity significantly [33]. Overall, blood-contacting medical devices must improve hemocompatibility in order to increase device function and patient health outcomes.

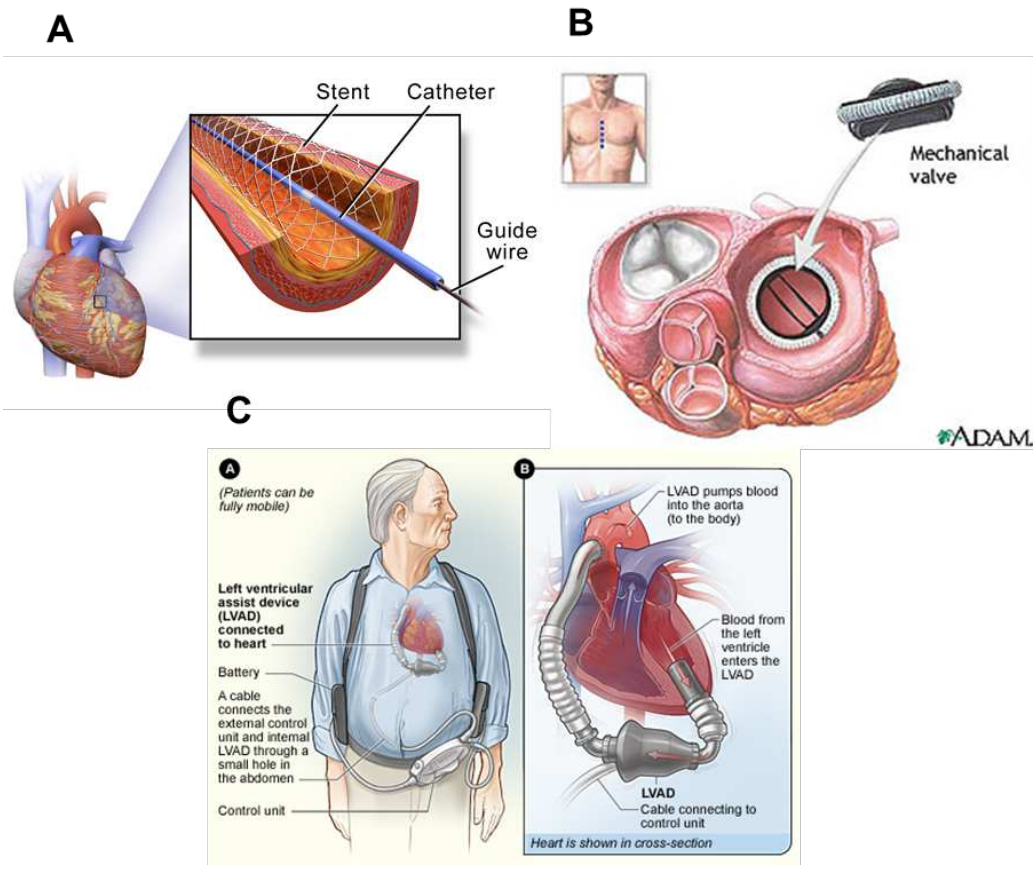

Figure 1.3.1: Examples of blood-contacting devices: (**A**) coronary stent, (**B**) mechanical heart valve, and (**C**) a left ventricular assist device. (**A**) adapted with permission from Blausen.com staff (2014). "Medical gallery of Blausen Medical 2014". WikiJournal of Medicine. (**B**) and (**C**) adapted from the National Library of Medicine and the National Heart Lung and Blood Institute, respectively.

1.4 Bacterial infection on surfaces

Bacterial infection on medical devices can originate from contamination from medical personnel, surgical implantation, or the patient's own microflora. Hospital-acquired infections in the U.S. numbered roughly 687,000 in 2015, of which 72,000 resulted in patient death [34]. It is estimated that 60-70% of these infections are associated with an implanted medical device [35]. Bacterial infection has been observed on practically all medical devices, including blood-contacting devices like prosthetic heart valves, intravascular catheters, artificial hearts, LVADs, and vascular prostheses [35]. The threat of bacterial infection on these devices is a significant concern in the short and long-term, as patients can have chronic and recurring infections [36–38].

Bacterial adhesion on a device surface often leads to the formation of a biofilm, a protective layer composed primarily of proteins and polysaccharides that makes treatment with antibiotics incredibly difficult [39,40]. Common bacterial strains involved in infections are *Pseudomonas aeruginosa*, *Staphylococcus epidermidis*, and *Staphylococcus aureus* as they are excellent at forming biofilms [41–43]. Bacteria are often classified as either Gram-positive (e.g. *S. aureus*) or Gram-negative (e.g. *P. aeruginosa*), where the distinction in cell wall can be determined through Gram-staining [44]. Gram-positive bacteria have a thick (15-80 nm) peptidoglycan layer on top of a phospholipid-rich cytoplasmic membrane, whereas Gram-negative bacteria have a thin (1-2 nm) peptidoglycan layer sandwiched between an inner and outer cytoplasmic membrane [45]. Bacterial cells of both bacterial types exist in two distinct forms. One form is the planktonic state, where the bacteria are free-floating, and the other is the sessile state, where bacteria are adhered to a surface. The sessile state is the state of bacteria in a biofilm and is commonly the focus of recent antibacterial research.

The first step in biofilm development is the rapid deposition of a conditioning film on the device surface from the natural aqueous medium (blood, saliva, urine, etc.) [40,46]. These films consist of glycoproteins and proteins such as fibrinogen, fibronectin, vitronectin, and albumin, which serve as binding ligands for bacterial receptors [35,40]. The binding of these film components to the surface can be affected by surface factors like surface chemistry, charge, and hydrophobicity [40]. The next step is cell deposition by a variety of different transport mechanisms, both physical and chemical [35,47,48]. Physical forces that move or attract bacterial to a surface include Brownian motion, Van Der Waals attraction, gravitational forces, electrostatics, surface charge, and hydrophobic interactions [48]. Diffusible chemical attractants (e.g. amino acids, sugars, and oligopeptides) occur in nearly all microbes and can direct bacterial movement [48]. Once bacteria are within a very short range of the surface (<1.5 nm) they adhere via chemical interactions mediated through physical appendages (e.g. fimbriae and capsules) [40,48]. For example, *S. epidermidis* use polysaccharide adhesins such as PS/A and SAA to adhere to

surfaces [48]. In addition, bacteria attach and interact with proteins deposited from the conditioning film [46,48]. Fibrinogen, which plays a vital role in coagulation, increases and strengthens adhesion of *S. aureus* to surfaces [49,50]. Fibronectin also promotes *S. aureus* adhesion [47]. If binding reactions to the surface are weak, bacteria may desorb back into the aqueous medium [51]. Several theoretical approaches have been proposed to explain and predict the physicochemical interactions that govern the adhesion of bacteria to surfaces. Examples of this include DLVO theory, which describes the net interaction between a cell and a surface as a balance between forces, and thermodynamic theory, which attempts to assign values of surface free energy to cell and surface components [48]. Although these frameworks aid in describing adhesion of bacteria to cells, they were originally applied to non-biological transport systems, and thus cannot fully account for the multitude of additional biological and surface factors.

Once cells are securely attached to a surface, cell-cell signaling facilitates the production of extracellular polymeric substances (EPS), which may compose 50-90% of the total organic carbon of a biofilm and consists mainly of polysaccharides [46,51]. Communication between bacterial cells is achieved through diffusible chemical signal molecules, so-called autoinducers, a process dubbed quorum sensing. Quorum sensing processes occur in both Gram-negative and Gram-positive bacteria, although their mechanisms often differ. Studies with *P. aeruginosa* suggest quorum sensing plays a significant role in the formation of biofilms through the *las* gene-regulatory system and other quorum circuits aid in the development of virulence (host-infecting) factors such as exoproteases, siderophores, exotoxins and rhamnolipids [52]. Gram-positive bacterial strains often use peptide-mediated systems for quorum sensing [52]. The *agr* regulatory system is central to cell attachment, biofilm dispersal, chronic infection, and the secretion of virulence factors in biofilms of Gram-positive bacteria [52]. Complex cell-cell interactions in both bacterial types lead to a matured 3D biofilm with increased EPS production, cell aggregation, formation of macro and microcolonies, and the transportation of nutrients [43,51]. In addition, outside host cells, such as platelets, can become absorbed into the biofilm matrix [51]. Finally,

dispersion of a mature biofilm can occur through either passive or active means [53,54]. Passive methods of dispersion include external factors like shear forces and collision with other solid components. Active processes often involve the production of enzymes made from glycosidases, proteases, and deoxyribonucleases that can break down the biofilm matrix or substrate material [53]. Detached biofilms may travel and begin colonizing a different location on a surface, which leads to recurring infections. Therefore, biomaterials that effectively impede biofilm formation would drastically reduce the occurrence of bacterial infection.

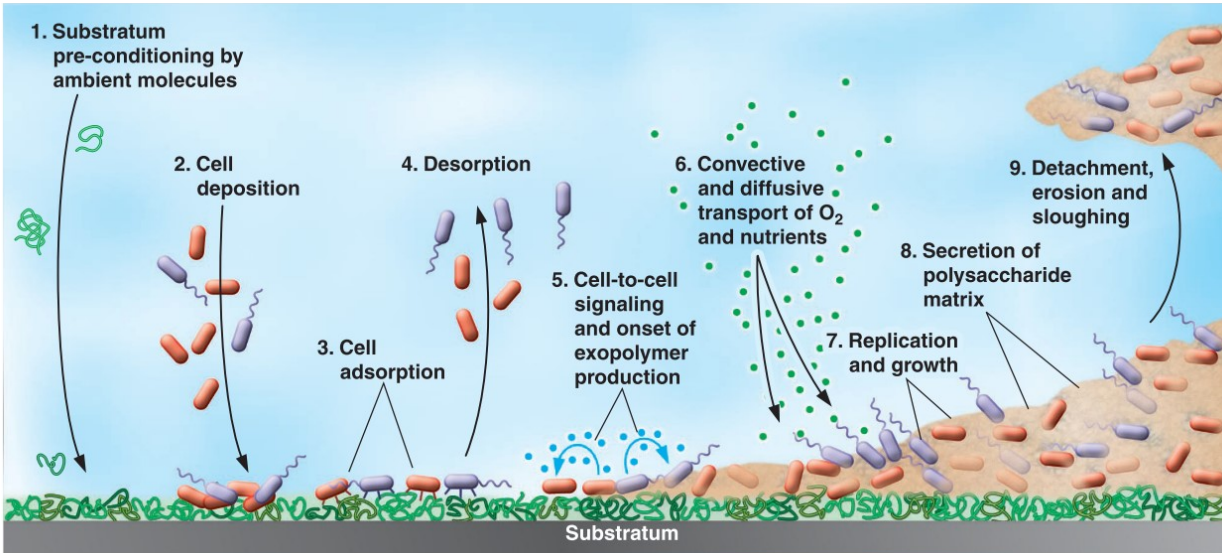

Figure 1.4.1: The processes of biofilm formation on device surfaces. Adapted with permission from the American Society for Microbiology: [ASM News Vol. 70 N. 5] J. Bryers, Ratner BD, Bioinspired implant materials befuddle bacteria. Copyright (2004). License at https://creativecommons.org/licenses/by-nc-sa/3.0/ [51].

1.5 Current solutions for thrombosis and bacterial infection on biomedical devices

Today, antiplatelet agents are frequently used for the prevention and treatment of thrombosis on blood-contacting devices. One example of this is DAPT, which is required following DES implantation. DAPT is a combination of aspirin and a P2Y12 receptor inhibitor such as clopidogrel, prasugrel, or ticagrelor [55]. Aspirin inhibits platelet aggregation by suppressing cyclooxygenase (COX) activity, a set of enzymes that lead to the production of thromboxane A_2 by activated platelets [56]. Although aspirin is effective for the prevention of thrombosis, it is also

linked to bleeding in the gastrointestinal tract and even drug resistance in up to 40% of patients [27,56,57]. Clopidogrel and prasugrel are drugs known as thienopyridines that, once metabolized, act to inhibit ADP-induced platelet aggregation by binding to the P2Y12 platelet receptor [56]. In contrast, ticagrelor is a drug that directly acts to inhibit the P2Y12 platelet receptor [58]. Ticagrelor is considered more effective than clopidogrel, which is commonly used, but may increase risk of patient bleeding as well [58]. DAPT is often chosen over aspirin-only treatment as it is proven more effective [56,59]. Regardless of the specific drugs prescribed, DAPT is usually recommended for 6-12 months, yet research suggests DAPT beyond 1 year may be necessary to prevent thrombosis [59]. Anticoagulants used in combination with antiplatelet therapies or singularly are also administered to combat thrombosis. Classic anticoagulants include heparin, which blocks thrombin and FXa via antithrombin, and vitamin K antagonists (VKAs) like warfarin, which block the production of several critical clotting factors [16]. A drawback of these anticoagulants is the need of close monitoring to ensure a therapeutic level of anticoagulation [16]. Low-molecular weight heparin (LMWH) and fondaparinux are anticoagulants developed to circumvent this requirement, yet they proved to be less effective and non-reversible [16]. Thus, heparin in ECMO procedures and VKAs after MHV and VAD procedures remain widely used [16,29].

Resistance to antibiotics is considered a significant and growing healthcare problem facing the world today [60]. Furthermore, biofilms appear to resist antibiotics to a much greater degree than planktonic bacteria, which leads to chronic and recurring infections on implanted devices [61]. Bacteria in biofilms may obtain resistance through several different mechanisms. Among these are persister cells and efflux pumps. Persister cells are cells that outlast the effects of antimicrobial agents and reform biofilms after most other cells have been wiped out [62]. Efflux plumps are transport proteins that contribute heavily to multidrug resistance in Gram-negative bacteria by moving antimicrobial agents outside of the bacteria [62]. These and other mechanisms are formed or aided by genetic adaptation facilitated through cell-cell interactions and quorum

sensing [42,62,63]. Often times continued systemic antibiotic therapy and removal/replacement of implanted medical devices is the only option for fighting bacterial infections [64]. Since treating developed biofilms has become an increasingly difficult task, most current researchers are looking toward surface modification to combat the adhesion of planktonic bacteria that cause biofilms.

Surface modifications of biomaterials offer a solution to surface fouling by blood components and bacteria without the need for long-lasting and ineffective systemic drug therapies. Of the proposed surface modifications that reduce blood clotting, heparin coatings are one of the few that are commercially available today [65]. Heparin coatings act like the natural glycosaminoglycan heparan sulfate of blood vessels and are believed to promote activity of antithrombin [65,66]. They are often used in LVADs and extra-corporeal circuits. A downside of heparin coatings is their tendency to lose efficacy and a condition known as heparin-induced thrombocytopenia type II (HIT II), where the platelet count becomes severely reduced and thrombosis risk increases [65,67]. Other methods include polyethylene glycol (PEG) coatings, albumin coatings, and endothelial cell coatings, where endothelial cells are seeded onto a surface to attempt reendothelialization of the device [65,68]. The problems with these solutions often include susceptibility to environmental factors, inefficacy in in vivo models, and difficulty finding an effective scaffold, respectively. Nitric oxide (NO) release has recently been investigated for both its antithrombic and antibacterial effects [69–71]. NO is naturally occurring and helps to construct and maintain healthy blood vessels [70]. Studies show promise for the use of NO in biomaterials, yet in vivo application and long-term release of NO has not been established [70]. Surface modifications for reducing bacterial fouling include the local release of antibiotics and silver ions, among others [36,72,73]. Antibiotics like gentamycin have been successfully loaded onto polymer scaffolds, yet the concern over antibiotic resistance remains and release is only temporary [36]. Coatings that release silver ions enter bacterial cells and disrupt critical functions without inducing resistance [36]. Unfortunately, this disruption appears to transfer to mammalian cells. Silver ion toxicity attacks organs such as the lung, liver, and brain, and possibly causes

damage to DNA [72,74]. Thus, there remains a need for biomedical surfaces that safely combat fouling. Superhydrophobic surfaces strongly repel the aqueous media that contain blood components and bacteria, and are therefore a promising surface modification explored in recent research.

1.6 Superhydrophobic materials

The discovery of superhydrophobic materials in nature, such as the lotus leaf, has led to the development of biomimetic superhydrophobic surfaces that have countless scientific and engineering applications [75–79]. Materials are classified as hydrophobic if they have water contact angles of >90° and hydrophilic if they have contact angles of <90°. Superhydrophobic materials are defined as materials with a water contact angle of greater than 150° and roll-off (sliding) angles of less than 10°. Superhydrophobicity on artificial surfaces is brought about by an interplay between surface texture and surface energy, and the theoretical framework behind its effects can largely be described by the Young, Wenzel, and Cassie-Baxter wetting models [80–82]. In general, the contact angle (θ) on a surface droplet is related to the surface tension of its solid, liquid, and vapor interfaces using Young's equation [80]:

$$\cos\theta = \frac{\gamma_{SV} - \gamma_{SL}}{\gamma_{LV}} \quad \textbf{(1-1)}$$

where γ is surface energy per unit surface area of the interfaces of solid (S), liquid (L), and vapor (V) phases. However, Young's equation does not account for surface roughness. Thus, Wenzel developed a modified Young's equation in 1936 that incorporates a surface roughness parameter [81,83]:

$$\cos\theta_W = r\cos\theta \quad \textbf{(1-2)}$$

where θ_W is the apparent contact angle in the Wenzel state and r is the ratio of actual surface area to projected surface area (r=1 for a smooth surface and r>1 for a rough surface). The Wenzel state pre-supposes a homogeneous wetting state, where fluid molecules are directly in contact

with surface features [84]. However, when surface roughness increases sufficiently, a transition occurs where the droplet is supported by both surface feature protrusions and an air-film layer between protrusions that helps prevent full wetting [75]. This is called a heterogenous wetting state and is the basis of superhydrophobicity. The Cassie-Baxter wetting model incorporates this state into the following equation [75]:

$$\cos\theta_{CB} = f(1 + \cos\theta) - 1 \qquad \textbf{(1-3)}$$

where θ_{CB} is the apparent contact angle in the Cassie-Baxter state and f is the ratio of solid-liquid area to solid-liquid and liquid-air area at the solid-liquid interface. A depiction of all three wetting models is shown below (**figure 1.6.1**).

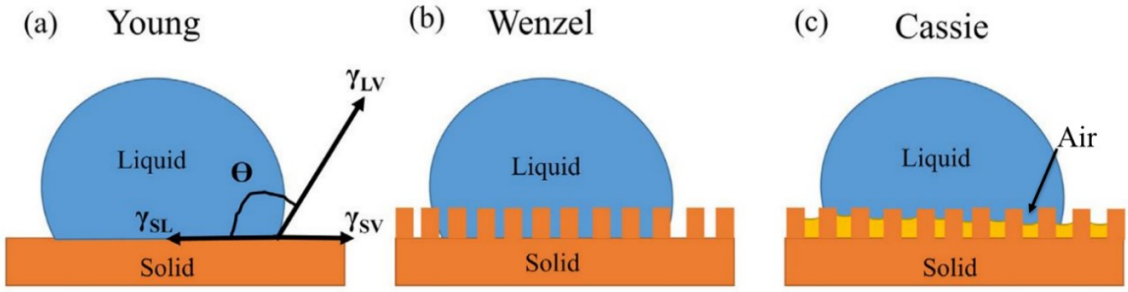

Figure 1.6.1: Depiction of (**A**) Young, (**B**) Wenzel, and (**C**) Cassie-Baxter wetting models. Adapted with permission from Elsevier B.V.: [Arabian Journal of Chemistry Vol. 13 Iss. 1] G. Barati Darband, M. Aliofkhazraei, S. Khorsand, S. Sokhanvar, A. Kaboli, Science and Engineering of Superhydrophobic Surfaces: Review of Corrosion Resistance, Chemical and Mechanical Stability. Copyright (2018). License at https://creativecommons.org/licenses/by-nc-nd/4.0/ [83].

Fabrication of superhydrophobic surfaces can be accomplished via a plethora of chemical and physical methods. These processes involve either roughing a low surface-energy surface or lowering the surface-energy of a roughened surface. Low surface-energy surfaces like fluorinated and perfluorinated silanes, phosphates, monomers, polymers, and copolymers are often selected for roughening, as they contain low surface-energy functional groups (e.g. $-CF_2$, $-CF_2H$, $-CF_3$, etc.) [85,86]. For example, poly(tetrafluoroethylene) (PTFE/Teflon) tape experiences a dramatic increase in water contact angle upon extension [87]. This is caused by an increased distance between fibrous crystals which essentially increases the amount of air between surface features.

Methods to fabricate rough surfaces that allow superhydrophobicity are varied. Etching with plasma, laser, and chemical methods are straightforward and effective for creating rough surfaces [86]. Lithography is also widely used to roughen surfaces and includes optical, nanoimprint, electron beam, X-ray, and colloidal methods [80]. Further methods to create rough surfaces include anodization, sol-gel processing, electrospinning, layer-by-layer self-assembly, and hydrothermal synthesis processes [86,88].

Rough surfaces become superhydrophobic by lowering surface energy, which is often accomplished with silanization. Silanization is a process whereby silane compounds are utilized to change the surface energy of a substrate (e.g. TiO_2, glass, metal, etc.). Silanes are used to modify surface properties such as adsorption and hydrophobicity/hydrophilicity. They are employed in a multitude of applications including optical coatings, architectural coatings, and anti-fog coatings [89]. The typical structure of a silane compound consists of an organofunctional group, linkage CH_2 groups, a silicone (Si) atom, and three hydrolysable groups [90]. The functional groups are what give the silane and consequently, the surface, its function. This generally entails low surface-energy fluorine groups like $-CF_2$ and $-CF_3$ in the case of superhydrophobic surfaces. The amount of linkage groups can be changed to customize the distance from the functional groups to the substrate, allowing molecular mobility [90]. The silane usually attaches to the surface via hydrolytic deposition, where the silicone atom covalently bonds to hydroxyl groups on the substrate surface. After successful bonding, a non-polar interphase and attached functional groups shield the polar surface from interactions with water [89]. An example of the silanization process is depicted below (**figure 1.6.2**).

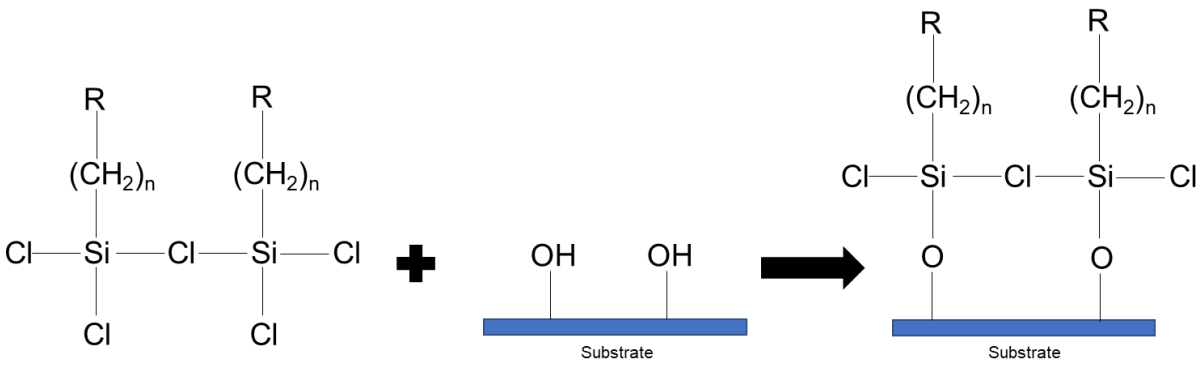

Figure 1.6.2: Example depiction of hydrolytic deposition of a trichlorosilane to a substrate.

The antiadhesive properties of superhydrophobic materials open the door to numerous applications including anti-icing [91], oil and water separation [92], drag reduction [93,94], desalination [95], and self-cleaning surfaces [83,96]. Furthermore, recent research on superhydrophobic surfaces shows promise for usage in biomedical devices, particularly blood-contacting biomedical devices. As mentioned previously, the deposition of blood-plasma proteins is a critical first step in thrombosis. Buffered by an air-film layer, superhydrophobic materials severely limit the amount of contact between blood-plasma and a device surface, reducing protein adsorption [75,97,98]. Reduced protein adsorption on a surface makes subsequent platelet adhesion and aggregation difficult since proteins, especially fibrinogen, play a significant role in these processes. Studies of superhydrophobic surfaces indicate reduced platelet adhesion in comparison to untextured and unmodified surfaces [99–102]. Reduction of initial thrombosis events then leads to reduced blood clotting and improved overall hemocompatibility [97,99]. In addition to reducing thrombosis, superhydrophobic materials have the potential to reduce adhesion and proliferation of bacteria. Bacterial adhesion is one of the first steps toward biofilms, which prove difficult to treat. Studies of superhydrophobic surfaces indicate reduced adhesion of both Gram-positive and Gram-negative bacteria compared to untextured and unmodified surfaces [39,103–106]. The mechanism that allows this is believed to be the same that prevents protein

adsorption (i.e. reduced surface contact leads to limited adhesion/adsorption). Although superhydrophobic surfaces show great potential in these applications, more research is needed to understand their capabilities and potential drawbacks. In addition, an appropriate material substrate must be used for fabricating a superhydrophobic surface. Titanium can form superhydrophobic surface coatings and may serve as a promising biocompatible substrate.

1.7 Titanium and titania nanomodification in biomaterials

Titanium and titanium alloys are well established as biomedical implants due to their good mechanical properties and high corrosion resistance [107]. Commercially pure titanium (CpTi) and alloys like Ti-6Al-4V have been used extensively in dental and orthopedic implants for more than 50 years [107]. In addition, titanium is used in cardiovascular devices such as prosthetic heart valves and artificial hearts as well as coronary stents in the form of nitinol [107]. Titanium's reactivity to oxygen creates a rapidly forming protective oxide (TiO_2/titania) layer when exposed to air. This layer is formed from the bulk titanium, meaning alloyed elements such as (Mo, Nb, V, etc.) are not significantly present on the surface [107]. The nanomodification of the titania layer has been the subject of research seeking to improve integration with various cellular environments. This has led to the fabrication of an assortment of titania nanotubes, nanorods, nanowires, nanopores, nanoleaves, nanoflowers, and more. Creation of titania nanotextures is often achieved through the same fabrication techniques that obtain roughness on superhydrophobic surfaces. One of the most common techniques is electrochemical anodization with a fluoride ion-containing electrolyte to create vertically aligned TiO_2 nanotube arrays with nanoscale features [108]. TiO_2 nanotubes exhibit improved osteoblast proliferation and adhesion due to the mimicking of real bone tissue by nano-scale surface features [107,109,110]. Titania nanotubes have also shown a decreased immune response after 7-day incubation in whole blood compared to unmodified titanium [111] and improved neural stem cell proliferation for neural prostheses [112]. Furthermore, titania nanotubes have been modified with various bioactive

components and indicate improved hemocompatibility and antibacterial activity [113]. Hydrothermal synthesis on Ti substrates is a simple and increasingly popular technique used to obtain titania nanostructures as well. Different chemical solutions containing NaOH, HF, H_2SO_4, etc. and applied heat etch the surface to create rough nanostructures. TiO_2 nanostructures fabricated via hydrothermal synthesis indicated improved endothelial cell function and hemocompatibility under static and dynamic conditions [114–116]. Similar titania nanostructures fabricated on stainless steel stents indicate improved reendothelialization, raised NO levels, and reduced vascular smooth muscles cell proliferation in vivo [117].

Thus, titania nanostructures have shown biocompatibility in several different cellular tissues. Furthermore, the combination of rough surface features and cellular compatibility makes titania nanostructures ideal for forming superhydrophobic surfaces. In fact, many of the hemocompatibility studies done to date on superhydrophobic surfaces have been fabricated on TiO_2 nanotubes. Superhydrophobic titania nanotubes indicated decreased fibrinogen and FXII adsorption, leading to improved hemocompatibility and antibacterial activity compared to control titanium surfaces [39,97,99]. Recently, superhydrophobic titania nanoflowers were fabricated and characterized with less platelet adhesion and activation than control surfaces [100]. This study demonstrated that other superhydrophobic titania nanostructures could have potential in biomedical applications. However, no other thrombosis related processes were investigated, nor the adhesion of bacteria. In addition, the properties of TiO_2 nanostructures fabricated on a Ti-6Al-4V substrate have not been characterized in the context of hemocompatibility. This alloy is used in bone implants and when high mechanical strength is needed, yet there is only one known study in the literature where superhydrophobic titania nanostructures were fabricated from Ti-6Al-4V substrate and investigated for hemocompatibility [118]. Therefore, for the first time, this work seeks to elucidate the hemocompatibility and bacterial adhesion characteristics of superhydrophobic titania nanoflowers fabricated on a Ti-6Al-4V substrate.

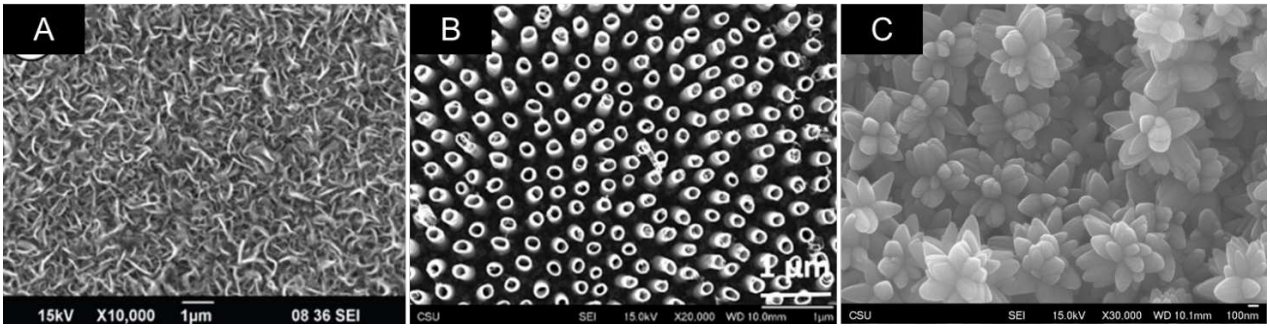

Figure 1.7.1: Examples of titania (**A**) nanoleaves, (**B**), nanotubes, and (**C**) nanoflowers. (**B**) and (**C**). (**A**) adapted with permission from John Wiley and Sons: [Advanced Healthcare Materials Vol. 6 Iss. 11] C.C. Mohan, A.M. Cherian, S. Kurup, J. Joseph, M.B. Nair, M. Vijayakumar, S. V. Nair, D. Menon, Stable Titania Nanostructures on Stainless Steel Coronary Stent Surface for Enhanced Corrosion Resistance and Endothelialization. Copyright (2017). [117]. (**B**) adapted with permission from The Royal Society of Chemistry: [RSC Advances Vol. 7] K. Bartlet, S. Movafaghi, A. Kota, K.C. Popat, Superhemophobic titania nanotube array surfaces for blood contacting medical devices. Copyright (2017). License at https://creativecommons.org/licenses/by-nc-sa/3.0/ [99].

REFERENCES

[1] I.H. Jaffer, J.C. Fredenburgh, J. Hirsh, J.I. Weitz, Medical device-induced thrombosis: what causes it and how can we prevent it?, J. Thromb. Haemost. 13 (2015) S72–S81. https://doi.org/10.1111/jth.12961.

[2] B. Savage, Z.M. Ruggeri, Selective Recognition of Adhesive Sites in Surface-bound Fibrinogen by Glycoprotein IIb-IIIa on Nonactivated Platelets, J. Biol. Chem. . 266 (1991) 11227–11233.

[3] W. Tsai, J.M. Grunkemeier, T.A. Horbett, Human plasma fibrinogen adsorption and platelet adhesion to polystyrene, J. Biomed. Mater. Res. 44 (1999) 130–139. https://doi.org/10.1002/(SICI)1097-4636(199902)44:2<130::AID-JBM2>3.0.CO;2-9.

[4] S.-H. Yun, E.-H. Sim, R.-Y. Goh, J.-I. Park, J.-Y. Han, Platelet Activation: The Mechanisms and Potential Biomarkers, Biomed Res. Int. 2016 (2016). https://doi.org/10.1155/2016/9060143.

[5] L. Tremolizzo, G. Sala, C. Ferrarese, Platelet Activation, in: Encycl. Psychopharmacol., Springer Berlin Heidelberg, Berlin, Heidelberg, 2010: pp. 1034–1035. https://doi.org/10.1007/978-3-540-68706-1_808.

[6] J.D. Loike, B. Sodeik, L. Cao, S. Leucona, J.I. Weitz, P.A. Detmers, S.D. Wright, S.C. Silverstein, CD11c/CD18 on neutrophils recognizes a domain at the N terminus of the Aα chain of fibrinogen, Proc. Natl. Acad. Sci. U. S. A. 88 (1991) 1044–1048. https://doi.org/10.1073/pnas.88.3.1044.

[7] S.D. Wright, J.I. Weitz, A.J. Huang, S.M. Levin, S.C. Silverstein, J.D. Loike, Complement receptor type three (CD11b/CD18) of human polymorphonuclear leukocytes recognizes fibrinogen, Proc. Natl. Acad. Sci. U. S. A. 85 (1988) 7734–7738. https://doi.org/10.1073/pnas.85.20.7734.

[8] C. Cerletti, C. Tamburrelli, B. Izzi, F. Gianfagna, G. De Gaetano, Platelet-leukocyte interactions in thrombosis, Thromb. Res. 129 (2012) 263–266. https://doi.org/10.1016/j.thromres.2011.10.010.

[9] P. Turbill, T. Beugeling, A.A. Poot, Proteins involved in the Vroman effect during exposure of human blood plasma to glass and polyethylene, Biomaterials. 17 (1996) 1279–1287. https://doi.org/10.1016/s0142-9612(96)80004-4.

[10] M. Sefton, I.H. Jaffer, J.I. Weitz, M. Gorbet, J.L. Brash, T.A. Horbett, R.A. Latour, P. Tengvall, C. Sperling, M.F. Maitz, C.A. Siedlecki, C. Werner, M.C. Martins, N. Grabow, C. Matschegewski, N. Huang, E.L. Chaikof, M.A. Barbosa, The Blood Compatibility Challenge, SSRN Electron. J. (2020). https://doi.org/10.2139/ssrn.3345274.

[11] U. Amara, D. Rittirsch, M. Flierl, U. Bruckner, A. Klos, F. Gebhard, J.D. Lambris, M. Huber-Lang, Interaction between the coagulation and complement system, Adv. Exp. Med. Biol. 632 (2008) 71–79. https://doi.org/10.1007/978-0-387-78952-1_6.

[12] M.J. Krisinger, V. Goebeler, Z. Lu, S.C. Meixner, T. Myles, E.L.G. Pryzdial, E.M. Conway, Thrombin generates previously unidentified C5 products that support the terminal complement activation pathway, Blood. 120 (2012) 1717–1725. https://doi.org/10.1182/blood-2012-02-412080.

[13] L.L. Swystun, P.C. Liaw, The role of leukocytes in thrombosis, Blood. 128 (2016) 753–762. https://doi.org/10.1182/blood-2016-05-718114.

[14] R.I. Litvinov, J.W. Weisel, Role of red blood cells in haemostasis and thrombosis, ISBT Sci. Ser. 12 (2017) 176–183. https://doi.org/10.1111/voxs.12331.

[15] J.R. Byrnes, A.S. Wolberg, Red blood cells in thrombosis, Blood. 130 (2017) 1795–1799. https://doi.org/10.1182/blood-2017-03-745349.

[16] I.H. Jaffer, J.I. Weitz, The blood compatibility challenge. Part 1: Blood-contacting medical devices: The scope of the problem, Acta Biomater. 94 (2019) 2–10. https://doi.org/10.1016/j.actbio.2019.06.021.

[17] J. Iqbal, J. Gunn, P.W. Serruys, Coronary stents: historical development, current status and future directions, Br. Med. Bull. 106 (2013). https://doi.org/10.1093/bmb/ldt009.

[18] CDC, Coronary Artery Disease, Cent. Dis. Control. (2019). https://www.cdc.gov/heartdisease/coronary_ad.htm (accessed May 21, 2020).

[19] R. Ross, Atherosclerosis — An Inflammatory Disease, N. Engl. J. Med. 340 (1999) 115–126. https://doi.org/10.1056/NEJM199901143400207.

[20] P. Libby, P.M. Ridker, A. Maseri, Inflammation and Atherosclerosis, Circulation. 105 (2002) 1135–1143. https://doi.org/10.1161/hc0902.104353.

[21] T. Schmidt, J. Abbott, Coronary Stents: History, Design, and Construction, J. Clin. Med. 7 (2018) 126. https://doi.org/10.3390/jcm7060126.

[22] E.S. Brilakis, V.G. Patel, S. Banerjee, Medical management after coronary stent implantation: A review, JAMA - J. Am. Med. Assoc. 310 (2013) 189–198. https://doi.org/10.1001/jama.2013.7086.

[23] D. He, W. Liu, T. Zhang, The development of carotid stent material., Interv. Neurol. 3 (2015) 67–77. https://doi.org/10.1159/000369480.

[24] G. Mani, M.D. Feldman, D. Patel, C.M. Agrawal, Coronary stents: A materials perspective, Biomaterials. 28 (2007) 1689–1710. https://doi.org/10.1016/J.BIOMATERIALS.2006.11.042.

[25] S. Garg, P.W. Serruys, Coronary stents: Current status, J. Am. Coll. Cardiol. 56 (2010) S1–S42. https://doi.org/10.1016/j.jacc.2010.06.007.

[26] D.R. Holmes, D.J. Kereiakes, S. Garg, P.W. Serruys, G.J. Dehmer, S.G. Ellis, D.O. Williams, T. Kimura, D.J. Moliterno, Stent Thrombosis, J. Am. Coll. Cardiol. 56 (2010) 1357–1365. https://doi.org/10.1016/J.JACC.2010.07.016.

[27] G.J. Hankey, J.W. Eikelboom, Aspirin resistance, Lancet. 367 (2006) 606–617. https://doi.org/10.1016/S0140-6736(06)68040-9.

[28] Price T.E., Schuchat A., Rothwell C., Health United States Report 2016, 2016.

[29] G.D. Dangas, J.I. Weitz, G. Giustino, R. Makkar, R. Mehran, Prosthetic Heart Valve Thrombosis, J. Am. Coll. Cardiol. 68 (2016) 2670–2689. https://doi.org/10.1016/j.jacc.2016.09.958.

[30] AHA, Types of Replacement Heart Valves, Am. Hear. Assoc. (2020). https://www.heart.org/en/health-topics/heart-valve-problems-and-disease/understanding-

your-heart-valve-treatment-options/types-of-replacement-heart-valves (accessed June 3, 2020).

[31] J. Luszczak, A. Undas, M. Gissel, M. Olszowska, S. Butenas, Activated factor XI and tissue factor in aortic stenosis: Links with thrombin generation, Blood Coagul. Fibrinolysis. 22 (2011) 473–479. https://doi.org/10.1097/MBC.0b013e328346c2bb.

[32] R.C. Starling, N. Moazami, S.C. Silvestry, G. Ewald, J.G. Rogers, C.A. Milano, J.E. Rame, M.A. Acker, E.H. Blackstone, J. Ehrlinger, L. Thuita, M.M. Mountis, E.G. Soltesz, B.W. Lytle, N.G. Smedira, Unexpected Abrupt Increase in Left Ventricular Assist Device Thrombosis, N. Engl. J. Med. 370 (2014) 33–40. https://doi.org/10.1056/NEJMoa1313385.

[33] H.J. Dalton, P. Garcia-Filion, R. Holubkov, F.W. Moler, T. Shanley, S. Heidemann, K. Meert, R.A. Berg, J. Berger, J. Carcillo, C. Newth, R. Harrison, A. Doctor, P. Rycus, J.M. Dean, T. Jenkins, C. Nicholson, Association of bleeding and thrombosis with outcome in extracorporeal life support, Pediatr. Crit. Care Med. 16 (2015) 167–174. https://doi.org/10.1097/PCC.0000000000000317.

[34] CDC, HAI and Antibiotic Use Prevalence Survey | Emerging Infections Program | HAI | CDC, Centers Dis. Control Prev. (2015). https://www.cdc.gov/hai/eip/antibiotic-use.html (accessed May 28, 2020).

[35] J.D. Bryers, Medical biofilms, Biotechnol. Bioeng. 100 (2008) 1–18. https://doi.org/10.1002/bit.21838.

[36] K. Vasilev, J. Cook, H.J. Griesser, Antibacterial surfaces for biomedical devices, Expert Rev. Med. Devices. 6 (2009) 553–567. https://doi.org/10.1586/erd.09.36.

[37] R.O. Darouiche, Device-Associated Infections: A Macroproblem that Starts with Microadherence, Clin. Infect. Dis. 33 (2001) 1567–1572. https://doi.org/10.1086/323130.

[38] R.M. Donlan, Biofilms and device-associated infections, in: Emerg. Infect. Dis., Centers for Disease Control and Prevention (CDC), 2001: pp. 277–281. https://doi.org/10.3201/eid0702.010226.

[39] K. Bartlet, S. Movafaghi, L.P. Dasi, A.K. Kota, K.C. Popat, Antibacterial activity on superhydrophobic titania nanotube arrays, Colloids Surfaces B Biointerfaces. 166 (2018) 179–186. https://doi.org/10.1016/j.colsurfb.2018.03.019.

[40] M. Habash, G. Reid, Microbial biofilms: Their development and significance for medical device-related infections, J. Clin. Pharmacol. 39 (1999) 887–898. https://doi.org/10.1177/00912709922008506.

[41] E.B.M. Breidenstein, C. de la Fuente-Núñez, R.E.W. Hancock, Pseudomonas aeruginosa: All roads lead to resistance, Trends Microbiol. 19 (2011) 419–426. https://doi.org/10.1016/j.tim.2011.04.005.

[42] C.R. Arciola, D. Campoccia, P. Speziale, L. Montanaro, J.W. Costerton, Biofilm formation in Staphylococcus implant infections. A review of molecular mechanisms and implications for biofilm-resistant materials, Biomaterials. 33 (2012) 5967–5982. https://doi.org/10.1016/j.biomaterials.2012.05.031.

[43] Z. Khatoon, C.D. McTiernan, E.J. Suuronen, T.F. Mah, E.I. Alarcon, Bacterial biofilm formation on implantable devices and approaches to its treatment and prevention, Heliyon. 4 (2018) e01067. https://doi.org/10.1016/j.heliyon.2018.e01067.

[44] T. Gregersen, Rapid method for distinction of gram-negative from gram-positive bacteria, Eur. J. Appl. Microbiol. Biotechnol. 5 (1978) 123–127. https://doi.org/10.1007/BF00498806.

[45] A.T. Poortinga, R. Bos, W. Norde, H.J. Busscher, Electric double layer interactions in bacterial adhesion to surfaces, Surf. Sci. Rep. 47 (2002) 1–32.

[46] R.M. Donlan, Biofilms: Microbial life on surfaces, Emerg. Infect. Dis. 8 (2002) 881–890. https://doi.org/10.3201/eid0809.020063.

[47] Y.H. An, R.J. Friedman, Concise review of mechanisms of bacterial adhesion to biomaterial surfaces, J. Biomed. Mater. Res. 43 (1998) 338–348. https://doi.org/10.1002/(SICI)1097-4636(199823)43:3<338::AID-JBM16>3.0.CO;2-B.

[48] M. Katsikogianni, Y.F. Missirlis, CONCISE REVIEW OF MECHANISMS OF BACTERIAL ADHESION TO BIOMATERIALS AND OF TECHNIQUES USED IN ESTIMATING BACTERIAMATERIAL INTERACTIONS, Eur. Cells Mater. 8 (2004) 37–57. https://doi.org/10.22203/eCM.v008a05.

[49] R.B. Dickinson, J.A. Nagel, D. McDevitt, T.J. Foster, R.A. Proctor, S.L. Cooper, Quantitative comparison of clumping factor- and coagulase-mediated Staphylococcus aureus adhesion to surface-bound fibrinogen under flow, Infect. Immun. 63 (1995) 3143–3150. https://doi.org/10.1128/iai.63.8.3143-3150.1995.

[50] R.B. Dickinson, J.A. Nagel, R.A. Proctor, S.L. Cooper, Quantitative comparison of shear-dependent Staphylococcus aureus adhesion to three polyurethane ionomer analogs with distinct surface properties, J. Biomed. Mater. Res. 36 (1997) 152–162. https://doi.org/10.1002/(SICI)1097-4636(199708)36:2<152::AID-JBM3>3.0.CO;2-J.

[51] J. Bryers, Ratner BD, Bioinspired implant materials befuddle bacteria, ASM News. (2004). ftp://128.171.151.230/bhowe/outgoing/AMM/ALOHA_Mooring/ALOHA Mooring/Biofilm/Bryers_Ratner_Biofilm_article.pdf (accessed June 1, 2020).

[52] Y.-H. Li, X. Tian, Quorum Sensing and Bacterial Social Interactions in Biofilms, Sensors. 12 (2012) 2519–2538. https://doi.org/10.3390/s120302519.

[53] J.B. Kaplan, Biofilm Dispersal: Mechanisms, Clinical Implications, and Potential Therapeutic Uses, J. Dent. Res. 89 (2010) 205–218. https://doi.org/10.1177/0022034509359403.

[54] P. Gupta, S. Sarkar, B. Das, S. Bhattacharjee, P. Tribedi, Biofilm, pathogenesis and prevention—a journey to break the wall: a review, Arch. Microbiol. 198 (2016) 1–15. https://doi.org/10.1007/s00203-015-1148-6.

[55] G. Magnani, M. Valgimigli, Dual antiplatelet therapy after drug-eluting stent implantation, Interv. Cardiol. Rev. 11 (2016) 51–53. https://doi.org/10.15420/icr.2015:17:2.

[56] J.W. Eikelboom, J. Hirsh, F.A. Spencer, T.P. Baglin, J.I. Weitz, Antiplatelet drugs - Antithrombotic therapy and prevention of thrombosis, 9th ed: American College of Chest Physicians evidence-based clinical practice guidelines, Chest. 141 (2012) e89S-e119S. https://doi.org/10.1378/chest.11-2293.

[57] E.S. Huang, L.L. Strate, W.W. Ho, S.S. Lee, A.T. Chan, Long-term use of aspirin and the risk of gastrointestinal bleeding, Am. J. Med. 124 (2011) 426–433. https://doi.org/10.1016/j.amjmed.2010.12.022.

[58] L. Wallentin, R.C. Becker, A. Budaj, C.P. Cannon, H. Emanuelsson, J. Horrow, S. Husted, S. James, H. Katus, K.W. Mahaffey, B.M. Scirica, A. Skene, G. Steg, R.F. Storey, R.A. Harrington, S. Uppsala, Ticagrelor versus Clopidogrel in Patients with Acute Coronary Syndromes, N. Engl. J. Med. 361 (2009) 1045–57. https://doi.org/10.1056/NEJMoa0904327.

[59] L. Mauri, D.J. Kereiakes, R.W. Yeh, P. Driscoll-Shempp, D.E. Cutlip, P.G. Steg, S.-L.T. Normand, E. Braunwald, S.D. Wiviott, D.J. Cohen, D.R. Holmes, M.W. Krucoff, J. Hermiller, H.L. Dauerman, D.I. Simon, D.E. Kandzari, K.N. Garratt, D.P. Lee, T.K. Pow, P. Ver Lee, M.J. Rinaldi, J.M. Massaro, Twelve or 30 Months of Dual Antiplatelet Therapy after Drug-Eluting Stents, NEJM.Org. N Engl J Med. 23 (2014) 2155–66. https://doi.org/10.1056/NEJMoa1409312.

[60] J.M.A. Blair, M.A. Webber, A.J. Baylay, D.O. Ogbolu, L.J.V. Piddock, Molecular mechanisms of antibiotic resistance, Nat. Rev. Microbiol. 13 (2015) 42–51. https://doi.org/10.1038/nrmicro3380.

[61] P.S. Stewart, J.W. Costerton, Antibiotic resistance of bacteria in biofilms, Lancet. 358 (2001) 135–138. https://doi.org/10.1016/S0140-6736(01)05321-1.

[62] S. Singh, S.K. Singh, I. Chowdhury, R. Singh, Understanding the Mechanism of Bacterial Biofilms Resistance to Antimicrobial Agents, Open Microbiol. J. 11 (2017) 53–62. https://doi.org/10.2174/1874285801711010053.

[63] N. Høiby, T. Bjarnsholt, M. Givskov, S. Molin, O. Ciofu, Antibiotic resistance of bacterial biofilms, Int. J. Antimicrob. Agents. 35 (2010) 322–332. https://doi.org/10.1016/j.ijantimicag.2009.12.011.

[64] L.R. Rodrigues, Inhibition of bacterial adhesion on medical devices, Adv. Exp. Med. Biol. 715 (2011) 351–367. https://doi.org/10.1007/978-94-007-0940-9_22.

[65] M.F. Maitz, M.C.L. Martins, N. Grabow, C. Matschegewski, N. Huang, E.L. Chaikof, M.A. Barbosa, C. Werner, C. Sperling, The blood compatibility challenge. Part 4: Surface modification for hemocompatible materials: Passive and active approaches to guide blood-material interactions, Acta Biomater. 94 (2019) 33–43. https://doi.org/10.1016/j.actbio.2019.06.019.

[66] J.M. Whitelock, R. V. Iozzo, Heparan sulfate: A complex polymer charged with biological activity, Chem. Rev. 105 (2005) 2745–2764. https://doi.org/10.1021/cr010213m.

[67] P. Eghtesady, D. Nelson, S.M. Schwartz, D. Wheeler, J.M. Pearl, L.H. Cripe, P.B. Manning, Heparin-Induced Thrombocytopenia Complicating Support by the Berlin Heart, ASAIO J. 51 (2005) 820–825. https://doi.org/10.1097/01.mat.0000185630.83985.49.

[68] R. Gbyli, A. Mercaldi, H. Sundaram, K.A. Amoako, Achieving Totally Local Anticoagulation on Blood Contacting Devices, Adv. Mater. Interfaces. 5 (2018) 1700954. https://doi.org/10.1002/admi.201700954.

[69] Y. Zang, K.C. Popat, M.M. Reynolds, Nitric oxide-mediated fibrinogen deposition prevents platelet adhesion and activation, Biointerphases. 13 (2018). https://doi.org/10.1116/1.5042752.

[70] J.L. Harding, M.M. Reynolds, Combating medical device fouling, Trends Biotechnol. 32 (2014) 140–146. https://doi.org/10.1016/j.tibtech.2013.12.004.

[71] L. Paricio, B. Neufeld, M. Reynolds, Combined influence of nitric oxide and surface

roughness in biofilm reduction across bacteria strains, Biointerphases. 14 (2019). https://doi.org/10.1116/1.5089246.

[72] J. Hasan, R.J. Crawford, E.P. Ivanova, Antibacterial surfaces: the quest for a new generation of biomaterials, (n.d.). https://doi.org/10.1016/j.tibtech.2013.01.017.

[73] S. Taheri, A. Cavallaro, S.N. Christo, L.E. Smith, P. Majewski, M. Barton, J.D. Hayball, K. Vasilev, Substrate independent silver nanoparticle based antibacterial coatings, Biomaterials. 35 (2014) 4601–4609. https://doi.org/10.1016/j.biomaterials.2014.02.033.

[74] M. Ahamed, M.S. AlSalhi, M.K.J. Siddiqui, Silver nanoparticle applications and human health, Clin. Chim. Acta. 411 (2010) 1841–1848. https://doi.org/10.1016/j.cca.2010.08.016.

[75] E.J. Falde, S.T. Yohe, Y.L. Colson, M.W. Grinstaff, Superhydrophobic materials for biomedical applications, Biomaterials. 104 (2016) 87–103. https://doi.org/10.1016/J.BIOMATERIALS.2016.06.050.

[76] P. Zhang, F.Y. Lv, A review of the recent advances in superhydrophobic surfaces and the emerging energy-related applications, Energy. 82 (2015) 1068–1087. https://doi.org/10.1016/j.energy.2015.01.061.

[77] S. Nagappan, C.S. Ha, Emerging trends in superhydrophobic surface based magnetic materials: Fabrications and their potential applications, J. Mater. Chem. A. 3 (2015) 3224–3251. https://doi.org/10.1039/c4ta05078a.

[78] D. Helmer, N. Keller, F. Kotz, F. Stolz, C. Greiner, T.M. Nargang, K. Sachsenheimer, B.E. Rapp, Transparent, abrasion-insensitive superhydrophobic coatings for real-world applications, Sci. Rep. 7 (2017) 1–6. https://doi.org/10.1038/s41598-017-15287-8.

[79] J. Jeevahan, M. Chandrasekaran, G. Britto Joseph, R.B. Durairaj, G. Mageshwaran, Superhydrophobic surfaces: a review on fundamentals, applications, and challenges, J. Coatings Technol. Res. 15 (2018) 231–250. https://doi.org/10.1007/s11998-017-0011-x.

[80] Y.Y. Yan, N. Gao, W. Barthlott, Mimicking natural superhydrophobic surfaces and grasping the wetting process: A review on recent progress in preparing superhydrophobic surfaces, Adv. Colloid Interface Sci. 169 (2011) 80–105. https://doi.org/10.1016/j.cis.2011.08.005.

[81] R.N. Wenzel, Resistance of solid surfaces to wetting by water, Ind. Eng. Chem. 28 (1936) 988–994. https://doi.org/10.1021/ie50320a024.

[82] A.B.D. Cassie, S. Baxter, Wettability of porous surfaces, Trans. Faraday Soc. 40 (1944) 546. https://doi.org/10.1039/tf9444000546.

[83] G. Barati Darband, M. Aliofkhazraei, S. Khorsand, S. Sokhanvar, A. Kaboli, Science and Engineering of Superhydrophobic Surfaces: Review of Corrosion Resistance, Chemical and Mechanical Stability, Arab. J. Chem. 13 (2020) 1763–1802. https://doi.org/10.1016/j.arabjc.2018.01.013.

[84] A. Marmur, Wetting on hydrophobic rough surfaces: To be heterogeneous or not to be?, Langmuir. 19 (2003) 8343–8348. https://doi.org/10.1021/la0344682.

[85] A.K. Kota, G. Kwon, A. Tuteja, The design and applications of superomniphobic surfaces, NPG Asia Mater. 6 (2014) e109–e109. https://doi.org/10.1038/am.2014.34.

[86] M. Ma, R.M. Hill, Superhydrophobic surfaces, Curr. Opin. Colloid Interface Sci. 11 (2006) 193–202. https://doi.org/10.1016/j.cocis.2006.06.002.

[87] J. Zhang, J. Li, Y. Han, Superhydrophobic PTFE surfaces by extension, Macromol. Rapid Commun. 25 (2004) 1105–1108. https://doi.org/10.1002/marc.200400065.

[88] Z. Guo, W. Liu, B.L. Su, Superhydrophobic surfaces: From natural to biomimetic to functional, J. Colloid Interface Sci. 353 (2011) 335–355. https://doi.org/10.1016/j.jcis.2010.08.047.

[89] B. Arkles, Hydrophobicity, Hydrophilicity and Silane Surface Modification, Paint Coatings Mag. (2006).

[90] B. Arkles, Silane Coupling Agents Connecting Across Boundaries, 2014. http://www.kellychemical.com (accessed April 21, 2020).

[91] L. Cao, A.K. Jones, V.K. Sikka, J. Wu, D. Gao, Anti-Icing superhydrophobic coatings, Langmuir. 25 (2009) 12444–12448. https://doi.org/10.1021/la902882b.

[92] A.K. Kota, Y. Li, J.M. Mabry, A. Tuteja, Hierarchically structured superoleophobic surfaces with ultralow contact angle hysteresis, Adv. Mater. 24 (2012) 5838–5843. https://doi.org/10.1002/adma.201202554.

[93] R.J. Daniello, N.E. Waterhouse, J.P. Rothstein, Drag reduction in turbulent flows over superhydrophobic surfaces, Phys. Fluids. 21 (2009) 085103. https://doi.org/10.1063/1.3207885.

[94] J.P. Rothstein, Slip on Superhydrophobic Surfaces, Annu. Rev. Fluid Mech. 42 (2010) 89–109. https://doi.org/10.1146/annurev-fluid-121108-145558.

[95] Y. Fan, S. Chen, H. Zhao, Y. Liu, Distillation membrane constructed by TiO2 nanofiber followed by fluorination for excellent water desalination performance, Desalination. 405 (2017) 51–58. https://doi.org/10.1016/j.desal.2016.11.028.

[96] R. Fürstner, W. Barthlott, C. Neinhuis, P. Walzel, Wetting and self-cleaning properties of artificial superhydrophobic surfaces, Langmuir. 21 (2005) 956–961. https://doi.org/10.1021/la0401011.

[97] R.M. Sabino, K. Kauk, S. Movafaghi, A. Kota, K.C. Popat, Interaction of blood plasma proteins with superhemophobic titania nanotube surfaces, Nanomedicine Nanotechnology, Biol. Med. 21 (2019). https://doi.org/10.1016/j.nano.2019.102046.

[98] C.R. Hsiao, C.W. Lin, C.M. Chou, C.J. Chung, J.L. He, Surface modification of blood-contacting biomaterials by plasma-polymerized superhydrophobic films using hexamethyldisiloxane and tetrafluoromethane as precursors, Appl. Surf. Sci. 346 (2015) 50–56. https://doi.org/10.1016/j.apsusc.2015.03.208.

[99] K. Bartlet, S. Movafaghi, A. Kota, K.C. Popat, Superhemophobic titania nanotube array surfaces for blood contacting medical devices, R. Soc. Chem. Adv. 7 (2017) 35466–35476. https://doi.org/10.1039/c7ra03373g.

[100] S. Movafaghi, V. Leszczak, W. Wang, J.A. Sorkin, L.P. Dasi, K.C. Popat, A.K. Kota, Hemocompatibility of Superhemophobic Titania Surfaces, Adv. Healthc. Mater. (2016). https://doi.org/10.1002/adhm.201600717.

[101] T. Sun, H. Tan, D. Han, Q. Fu, L. Jiang, No platelet can adhere-largely improved blood compatibility on nanostructured superhydrophobic surfaces, Small. 1 (2005) 959–963. https://doi.org/10.1002/smll.200500095.

[102] Q. Huang, Y. Yang, R. Hu, C. Lin, L. Sun, E.A. Vogler, Reduced platelet adhesion and improved corrosion resistance of superhydrophobic TiO2-nanotube-coated 316L stainless steel, Colloids Surfaces B Biointerfaces. 125 (2015) 134–141. https://doi.org/10.1016/j.colsurfb.2014.11.028.

[103] B.J. Privett, J. Youn, S.A. Hong, J. Lee, J. Han, J.H. Shin, M.H. Schoenfisch, Antibacterial fluorinated silica colloid superhydrophobic surfaces, Langmuir. 27 (2011) 9597–9601. https://doi.org/10.1021/la201801e.

[104] M. Zhang, P. Wang, H. Sun, Z. Wang, Superhydrophobic Surface with Hierarchical Architecture and Bimetallic Composition for Enhanced Antibacterial Activity, Appl. Mater. Interfaces. 6 (2014) 22108–22115. https://doi.org/10.1021/am505490w.

[105] X. Zhang, L. Wang, E. Levänen, Superhydrophobic surfaces for the reduction of bacterial adhesion, RSC Adv. 3 (2013) 12003–12020. https://doi.org/10.1039/c3ra40497h.

[106] A.K. Epstein, T.S. Wong, R.A. Belisle, E.M. Boggs, J. Aizenberg, Liquid-infused structured surfaces with exceptional anti-biofouling performance, Proc. Natl. Acad. Sci. U. S. A. 109 (2012) 13182–13187. https://doi.org/10.1073/pnas.1201973109.

[107] M. Kulkarni, A. Mazare, P. Schmuki, A. Iglič, Biomaterial surface modification of titanium and titanium alloys for medical applications, in: Nanomedicine, 2014: pp. 111–136.

[108] V.B. Damodaran, D. Bhatnagar, V. Leszczak, K.C. Popat, Titania nanostructures: A biomedical perspective, RSC Adv. 5 (2015) 37149–37171. https://doi.org/10.1039/c5ra04271b.

[109] L. Zhao, S. Mei, P.K. Chu, Y. Zhang, Z. Wu, The influence of hierarchical hybrid micro/nano-textured titanium surface with titania nanotubes on osteoblast functions, Biomaterials. 31 (2010) 5072–5082. https://doi.org/10.1016/j.biomaterials.2010.03.014.

[110] K.C. Popat, L. Leoni, C.A. Grimes, T.A. Desai, Influence of engineered titania nanotubular surfaces on bone cells, Biomaterials. 28 (2007) 3188–3197. https://doi.org/10.1016/j.biomaterials.2007.03.020.

[111] B.S. Smith, P. Capellato, S. Kelley, M. Gonzalez-Juarrero, K.C. Popat, Reduced in vitro immune response on titania nanotube arrays compared to titanium surface, Biomater. Sci. 1 (2013) 322–332. https://doi.org/10.1039/c2bm00079b.

[112] J.A. Sorkin, S. Hughes, P. Soares, K.C. Popat, Titania nanotube arrays as interfaces for neural prostheses., Mater. Sci. Eng. C. Mater. Biol. Appl. 49 (2015) 735–745. https://doi.org/10.1016/j.msec.2015.01.077.

[113] R.M. Sabino, K. Kauk, L.Y.C. Madruga, M.J. Kipper, A.F. Martins, K.C. Popat, Enhanced hemocompatibility and antibacterial activity on titania nanotubes with tanfloc/heparin polyelectrolyte multilayers, J. Biomed. Mater. Res. - Part A. 108 (2020) 992–1005. https://doi.org/10.1002/jbm.a.36876.

[114] C.C. Mohan, P.R. Sreerekha, V. V. Divyarani, S. Nair, K. Chennazhi, D. Menon, Influence of titania nanotopography on human vascular cell functionality and its proliferation in vitro, J. Mater. Chem. (2012). https://doi.org/10.1039/c1jm13726c.

[115] C.C. Mohan, K.P. Chennazhi, D. Menon, In vitro hemocompatibility and vascular endothelial cell functionality on titania nanostructures under static and dynamic conditions for improved coronary stenting applications, Acta Biomater. (2013). https://doi.org/10.1016/j.actbio.2013.08.023.

[116] V.K. Manivasagam, K.C. Popat, In Vitro Investigation of Hemocompatibility of Hydrothermally Treated Titanium and Titanium Alloy Surfaces, ACS Omega. (2020) acsomega.0c00281. https://doi.org/10.1021/acsomega.0c00281.

[117] C.C. Mohan, A.M. Cherian, S. Kurup, J. Joseph, M.B. Nair, M. Vijayakumar, S. V. Nair, D. Menon, Stable Titania Nanostructures on Stainless Steel Coronary Stent Surface for Enhanced Corrosion Resistance and Endothelialization, Adv. Healthc. Mater. 6 (2017) 1601353. https://doi.org/10.1002/adhm.201601353.

[118] J.Y. Jiang, J.L. Xu, Z.H. Liu, L. Deng, B. Sun, S.D. Liu, L. Wang, H.Y. Liu, Preparation, corrosion resistance and hemocompatibility of the superhydrophobic TiO 2 coatings on biomedical Ti-6Al-4V alloys, Appl. Surf. Sci. 347 (2015) 591–595. https://doi.org/10.1016/j.apsusc.2015.04.075.

CHAPTER 2

FABRICATION AND CHARACTERIZATION OF TITANIA NANOFLOWER SURFACES

2.1 Introduction

The surface features of medical devices have a large effect on the compatibility of the device within the body. Recent research has focused on modifying surface features like topography, chemistry, and wettability to increase compatibility between devices and surrounding cell tissues. Titanium and its alloys are extensively used in medical devices due to their high corrosion resistance and ideal mechanical strength. The titania oxide layer of these materials can be modified with a hydrothermal synthesis procedure to obtain a rough nanoflower surface texture. This rough surface texture in combination with a low surface-energy silane compound allows the surface to obtain superhydrophobic properties with contact angles above 150°. These properties may allow the surface to prevent fouling by blood components and bacteria on blood-contacting biomedical devices. In this work, fabricated superhydrophobic titania nanoflower surfaces were evaluated for their surface morphology with SEM imaging, surface chemistry via XPS analysis, crystal structure via XRD analysis, and water contact angle via goniometry. Surface stability was evaluated after 4 weeks of incubation and subsequently characterized with goniometry and XPS analysis.

2.2 Materials and Methods

2.2.1 Fabrication of superhydrophobic titania nanoflower surfaces

Titania nanoflower surfaces were fabricated using a hydrothermal synthesis procedure on a titanium alloy, Ti-6Al-4V, as previously described in Wu et al [1]. Sections of titanium alloy Ti-6Al-4V were cut into 2.5 cm x 5 cm substrates and polished with 1200 grit sandpaper. The substrates were then sonicated in 100% acetone for 10 mins to remove surface contaminants. After sonication, the substrates were rinsed in de-ionized (DI) water and placed in an oxygen-

plasma chamber to further remove surface contaminants. Finally, the substrates were transferred to sealed Teflon (PTFE) containers with 20 mM hydrofluoric acid (HF) solution and placed on a hot plate set to 300˚C. After 8 hours, the treated substrates were rinsed with DI water, dried in nitrogen, and stored until needed. The substrates were further cut into 0.5 cm x 0.5 cm surfaces for all surface characterization and biological studies.

Superhydrophobic surfaces on titania nanoflowers were created using a simple vapor-phase silanization process with (heptadecafluoro-1,1,2,2-tetrahydrodecyl) trichlorosilane. Prior to silanization, surfaces were placed in a plasma chamber at 200 V in 10 cm^3/min of oxygen gas for 15 mins to form -OH groups on the surface. Subsequently, the surfaces were placed on a glass slide adjacent to 200 µL of silane on a hot plate in an enclosed chamber. The hot plate was then heated to 120˚C and left for one hour. Finally, the surfaces were rinsed in DI water and dried with nitrogen.

The following nomenclature will be used throughout this thesis for different surfaces: Ti-6Al-4V titanium alloy (Ti), titanium alloy after silanization (Ti-s), nanoflower surface (NF), and nanoflower surface after silanization (NF-s). Both Ti and Ti-s were considered as control surfaces for all studies.

2.2.2 Characterization of titania nanoflower surfaces

The surface topography was characterized using a JEOL JSM-6500F Field Emission SEM. Prior to analysis, surfaces were coated with a 10 nm layer of gold to provide a conductive layer for imaging. Surfaces were imaged using 10kV at 6,500x, and 30,000x magnifications.

The surface chemistry was characterized with a PE-5800 XPS machine. Survey spectra were collected from 0 to 1100 eV and peak-fit analysis was done using Multipack and OriginLab software.

The surface crystal structure was characterized using a Shimadzu XRD 7000 maxima machine. XRD was carried out using Cu Kα radiation, thin film geometry with 2° incidence, a speed of 1°/min, and a range of 20 to 80 degrees.

The static contact-angle and roll-off angles of surfaces were measured using a Ramé-Hart Model 250 goniometer connected to a camera [2]. The surfaces were placed on the goniometer's stage where a 10 µL droplet of water was placed on top. Using the DROPimage software connected to the goniometer, the contact angle between the droplet and surface was measured. Roll-off angle was measured by tilting the stage with droplet still on the surface until it slid.

The surface stability was evaluated by incubating surfaces in 2 mL of phosphate-buffered saline (PBS) at 37˚C and 5% CO_2 on a shaker plate set to 100 rpm. and characterizing them using contact angle and surface chemistry analysis. A control set of surfaces was also exposed to ambient air at 37˚C and 5% CO_2 and evaluated similarly. The static contact-angles of the surfaces were measured initially and then subsequently every 7 days over a 4-week period using the method for characterizing surface wettability described above. XPS survey scans were taken initially and after the 4-week period using the method to characterize the surface chemistry described above.

2.2.3 Statistical analysis

Surface characterizations with SEM were done using at least 3 different surfaces for each surface type at 5 different locations on the surface (n_{min}=15). Surface characterizations with contact angles were done with at least 3 different surfaces for each surfaces type at 3 different locations on the surface (n_{min}=9). Statistical one-way ANOVA and student t-tests were completed for all quantitative results. Results were considered statistically significant with a p-value ≤ 0.05. Analysis was done using JMP and OriginLab software.

2.3 Results and Discussion

2.3.1 Surface characterization

The goal of this work was to develop a surface for a blood-contacting medical device with the ability to improve hemocompatibility and reduce bacterial adhesion. In recent years, researchers have shown the potential of using superhydrophobic surfaces for these applications [2–7]. To date, much of the research in this area has been done with titania nanotubes grown on CpTi using anodization. The intriguing results from these studies have inspired research into other titania nanotextures [8–10]. In 2016, Sanli et al. studied platelet adhesion and activation on titania nanoflower surfaces grown on CpTi [10]. The results indicated that the surface had reduced platelet adhesion and activation compared to untextured titanium; however, there was no extensive characterization of other critical thrombosis-related processes such as protein adsorption, leukocyte adhesion, and whole blood clotting. In addition, the behavior of bacterial adhesion on the surface remained unknown. For these reasons, further characterization of the surface is needed to fully understand its capabilities.

In this study, NF-s was fabricated on titanium alloy Ti-6Al-4V, instead of CpTi. This alloy has been extensively used in bone-related biomedical implants due to its high yield strength in comparison to CpTi and biocompatibility with bone tissues [11–14]. However, Ti-6Al-4V has not been thoroughly investigated with relation to hemocompatible titania nanosurfaces or superhydrophobic coatings and thus was chosen for this research. NF-s was fabricated using two primary chemical processes: hydrothermal synthesis and vapor-phase silanization. The hydrothermal synthesis process is outlined completely by Wu et al. [1] and is described by the following chemical equations. Initially, the Ti from the Ti-6Al-4V substrate reacts with HF to form H_2TiF_6.

$$Ti + 6HF \rightarrow H_2TiF_6 + 2H_2\uparrow \quad \textbf{(2-1)}$$

The H_2TiF_6 produced from this reaction then reacts with water molecules to create $Ti(OH)_4$.

$$H_2TiF_6 + 4H_2O \rightarrow Ti(OH)_4 + 6HF \quad \textbf{(2-2)}$$

The $Ti(OH)_4$ becomes TiO_2, nucleates, and continues to form more TiO_2 under reaction conditions.

$$Ti(OH)_4 \rightarrow TiO_2 + 2H_2O \quad \textbf{(2-3)}$$

The HF in solution begins to etch the formed TiO_2 while H_2TiF_6 diffuses to the surface of the TiO_2 nanoparticles, where more TiO_2 is continually created and deposited on top of itself [15].

$$TiO_2 + 6HF \rightarrow H_2TiF_6 + 2H_2O \quad \textbf{(2-4)}$$

Once the synthesis of NF was complete, vapor-phase silanization was utilized to form a superhydrophobic surface. This process begins by treating the NF surfaces in an oxygen plasma chamber to form hydroxyl (OH^-) groups on the surface. The silicon within the silane forms strong covalent R-Si-O bonds with these groups in order to attach itself to the substrate [16]. The combination of low surface-energy $-CF_2$ and $-CF_3$ functional groups bonded to the silicon and the rough nanoflower texture allow the surface to obtain high contact angles via the Cassie-Baxter state [17]. Either this state or the Wenzel state is observed when a droplet is placed onto a surface. In the Wenzel state, the fluid molecule is fully in contact with the surface features. Surfaces in this state do not achieve contact angles of >150˚, which are indicative of a superhydrophobic surface. In the Cassie-Baxter state, fluid molecules are only in contact with a small fraction of the surface features and an air-film layer trapped between these features [17]. This significantly increases contact angle and reduces the liquid-surface interfacial area, which can reduce surface blood-clot formation and bacterial adhesion.

SEM was used to characterize the surface topography of titania nanoflower surfaces. The results for Ti indicate the expected topography (**figure 2.3.1**). The surface was relatively flat but showed streaks and scratches due to surface imperfections and processing. The results for NF showed many clusters of nanoflower formation uniformly distributed throughout the surface. Modifying both surfaces with silane to create Ti-s and NF-s did not change surface morphology upon SEM inspection. Average nanoflower diameter was determined by analyzing SEM images in ImageJ software. This was done by measuring a straight line drawn across the longest distance

on the feature. The results indicate an average diameter of 823.6 ± 163.6 nm for the nanoflowers and no significant difference in the size of nanoflowers on NF-s when compared to NF.

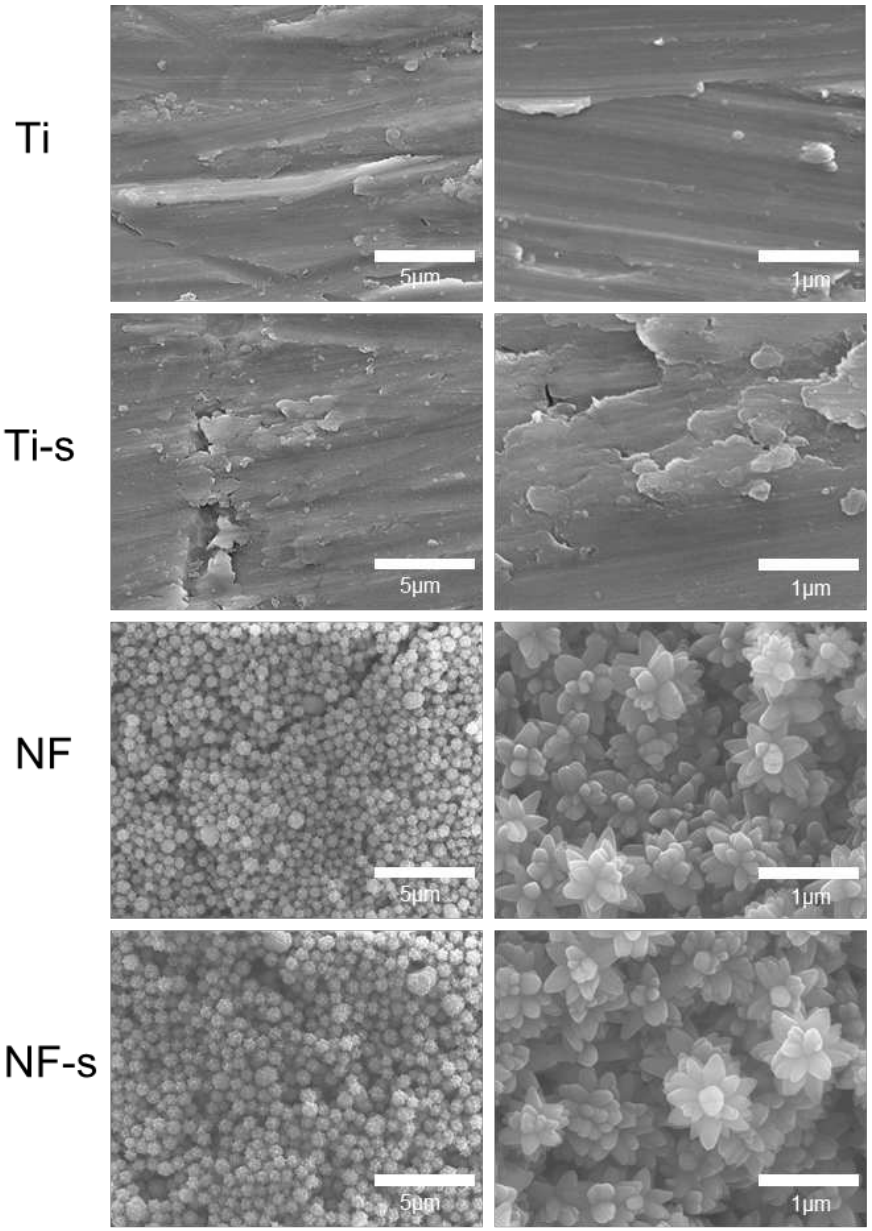

Figure 2.3.1: Representative SEM images of control and titania nanoflower surfaces fabricated using hydrothermal synthesis and vapor-phase silanization.

Contact angle and roll-off angle measurements were used to characterize surface wettability. Roll-off angles were found to be 29 ± 2.3˚ for Ti-s and 3 ± 0.5˚ for NF-s, while water droplets did not roll off Ti and NF. Ti, Ti-s, and NF, indicated the Wenzel state due to their relatively

low contact angles and wettability. Ti showed contact angles of <90° indicating the expected hydrophilic surface while Ti-s displayed contact angles of >90° indicating a hydrophobic surface. The silane coating lowered the surface energy and allowed it to obtain hydrophobic qualities; however, the lack of nanotexturing impeded the development of high contact angles typical of the Cassie-Baxter state. NF showed contact angles of approximately 0°, indicating a superhydrophilic surface. This was observed through complete surface wetting upon placing a droplet of water on the surface. Although the mechanisms of superhydrophilic surfaces are still under debate, the effect is generally apparent on rough surfaces, such as titania nanotextures, with large effective surface area compared to projected surface area [18]. Contact angle measurements on NF-s of >150° and roll-off angles of <10° confirmed the successful fabrication of a superhydrophobic surface. This indicates the presence of an air-film layer trapped between the surface features, and thus the Cassie-Baxter state.

XPS scans were used to characterize the surface chemistry. XPS scans indicate relative atomic composition on a surface by measuring atomic binding energy. The results indicated O1s, $Ti2p_{2/3}$, and C1s peaks on all surfaces (**figure 2.3.2**). F1s peaks and trace amounts of silicon in the form of Si2p peaks were visible on Ti-s and NF-s due to silanization. A smaller F1s peak was seen on the NF surface because of the presence of HF in the hydrothermal synthesis process. The O1s peak increase and subsequent $Ti2p_{2/3}$ peak decrease seen on NF was caused by oxidation from the hydrothermal synthesis process. The C1s peak was highest on Ti because of contamination present in the environment and on the surface. After silanization, there was a change of the shape of the C1s peaks on Ti-s and NF-s due to the $-CF_2$ and $-CF_3$ functional groups contained within the silane compound.

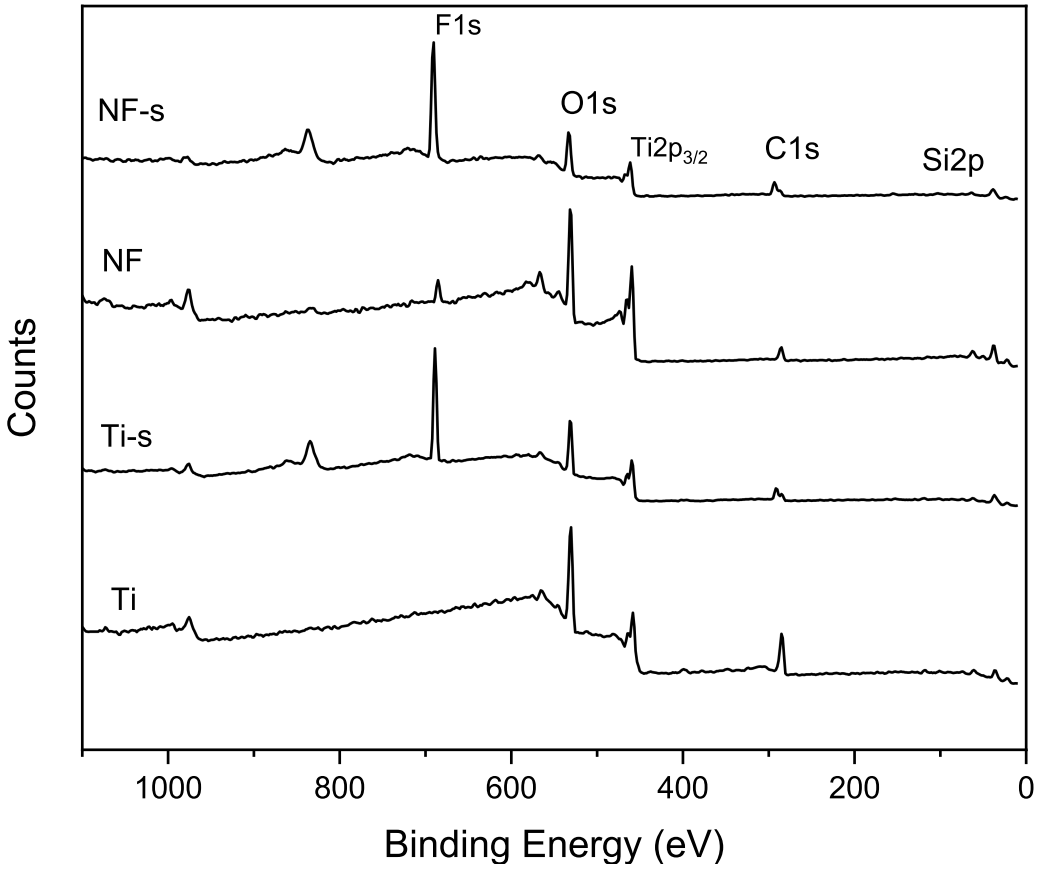

Figure 2.3.2: XPS survey scans for Ti, Ti-s, NF, and NF-s surfaces.

XRD was used to characterize the surface crystalline structure of different surfaces. Characterizing crystalline structure is useful for understanding the effects of hydrothermal synthesis and silanization on the titanium alloy surface. The results indicate the presence of rutile and anatase crystal phases on all surfaces (**figure 2.3.3**). The rutile phase is visible in the range of 35-40˚, 53˚, and 75-80˚, while the anatase phase is visible around 63˚ and 71˚. Both Ti and Ti-s surfaces also showed anatase at around 27˚. The rutile phase is known to be the most stable phase and the anatase phase has been shown to be biocompatible with several different types of cells [19–21]. Overall, minimal changes in crystalline structure were seen after silanization or hydrothermal synthesis.

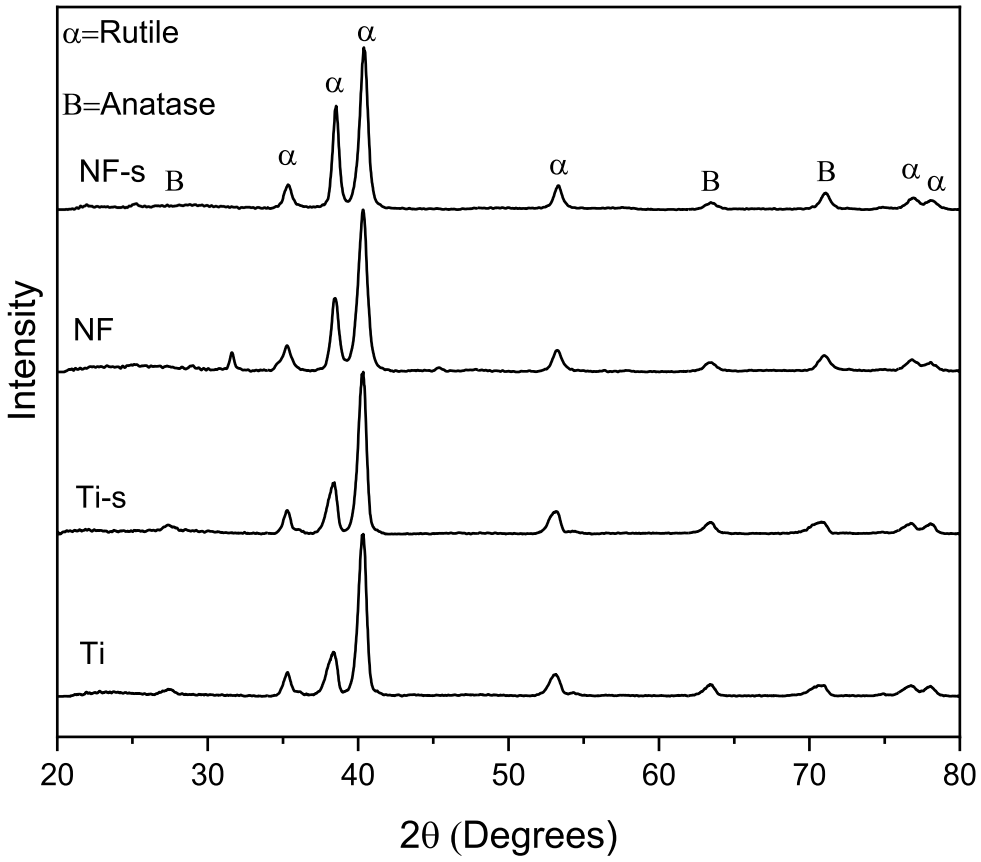

Figure 2.3.3: XRD scans of Ti, Ti-s, NF, and NF-s surfaces.

Surface stability plays a vital role in internal medical devices because the device may be implanted in a patient for many years. Surfaces composed of superhydrophobic nanotextures present a challenge in this area. If the air-film layer necessary to maintain the Cassie-Baxter state is compromised, then the surface will lose its superhydrophobic nature, which will increase interaction between blood components, bacteria, and the surface, leading to complications. Past research has shown air-film layers to be stable on superhydrophobic surfaces for at least 50 days under controlled parameters [22] and Sabino et al. showed titania nanotubes to be stable when incubated in PBS for 4 weeks under physiologically similar conditions [23]. In this work, stability was characterized after incubating surfaces in air or PBS under physiologically similar conditions for 4 weeks. The results indicate that after 4 weeks in air, Ti contact angles significantly increased

from 67.1 ± 4.6˚ to 87.8 ± 5.6˚ (31%) while Ti-s, NF, and NF-s contact angles remained as they were as-fabricated (p≤0.05) (**figure 2.3.4A**). This increase was not expected and was due to contamination on Ti. After 4 weeks in PBS, Ti and NF contact angles did not significantly change (**figure 2.3.4B**). Ti-s and NF-s both showed statistically significant decreases of 121.8 ± 7.0˚ to 94.3 ± 5.1˚ (23%) and 159.6 ± 3.7˚ to 154.5 ± 4.6˚ (3%) respectively (p≤0.05). However, NF-s maintained superhydrophobic contact angles of >150° after 4-week incubation in both cases, which was significantly higher than all other surfaces (p≤0.05).

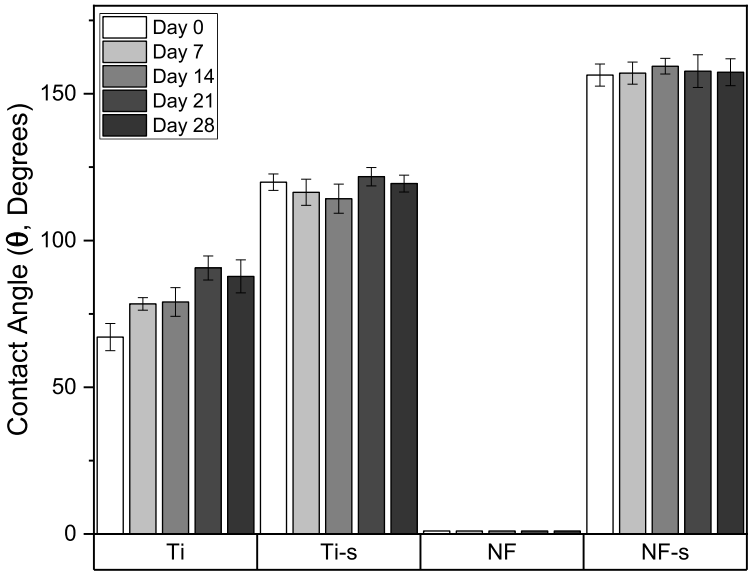

(**A**)

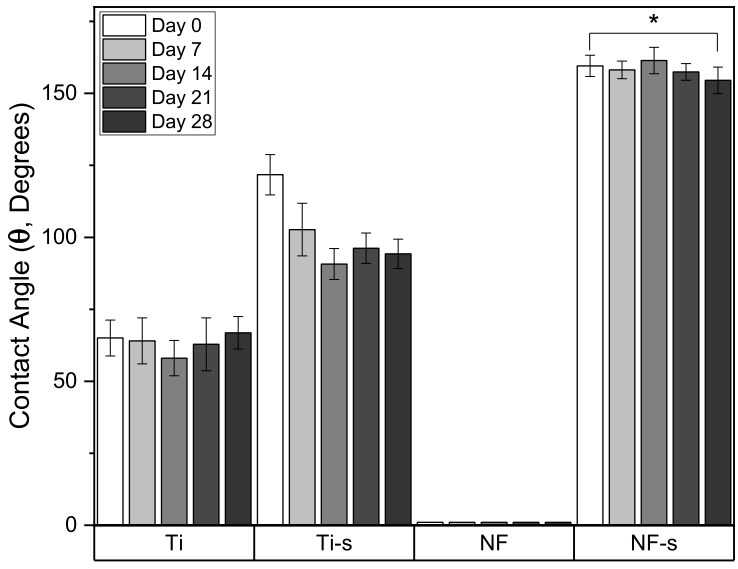

(**B**)

Figure 2.3.4: Contact angle measurements on Ti, Ti-s, NF, and NF-s surfaces incubated in air (**A**) and PBS (**B**) over a 4-week period. A slight decrease was seen in contact angle for NF-s in PBS ($p \leq 0.05$). Note: statistics are discussed further in results and discussion.

XPS survey scans (data not shown) were taken after the 4-week period for surfaces incubated in air or PBS. Quantized results for the survey scans were tabulated in **table 2.3.1**. The results indicate silicon and fluorine elemental composition on NF-s decreased after 4-week incubation in either air or PBS, suggesting a degradation of the silane coating that allows for a superhydrophobic surface. High resolution XPS C1s scans of the surfaces were taken to further investigate the degree of this degradation by observing the $-CF_2$ and $-CF_3$ functional groups that are characteristic of the silane. These scans indicate C-C (~284.8 eV) and C-O (~286.5 eV) functional groups were found on all surfaces (**figure 2.3.5**), and O-C=O (~288.5 eV) was detected on Ti, Ti-s, and NF. As expected, $-CF_2$ (~292.0 eV) and $-CF_3$ (~293-294 eV) functional groups were found on Ti-s and NF-s. The results obtained after 4-week incubation in PBS are of primary importance for evaluating surface stability because they model what may happen when implants are in contact with liquid media after an extended period. Looking closely at the $-CF_2$ and $-CF_3$ functional groups on Ti-s, a reduction in peak intensity is evident on the surface incubated in PBS in comparison to the as-fabricated and air-incubated surfaces. In contrast, these functional groups remained in similar quantities on NF-s under all conditions. These results explain why such a steep decrease in contact angle was seen after 4-week incubation on Ti-s compared to NF-s (**figure 2.3.4B**). Overall, the results suggest the nanotexture of NF-s allowed the surface to maintain the air-film layer, allowing high contact angles (>150°) and thus surface stability to remain.

Table 2.3.1: Elemental composition for as-fabricated, 4-week air, and 4-week PBS surfaces taken from XPS survey scans.

		F%	O%	Ti%	C%	Si%
As Fabricated	**Ti**	0.00	50.67	26.60	22.76	0.00
	Ti-s	53.20	19.96	16.78	9.56	0.56
	NF	7.92	61.44	13.46	17.17	0.00
	NF-s	45.23	22.21	6.99	23.56	2.01
Air	**Ti**	0.00	40.28	15.09	44.63	0.00
	Ti-s	53.61	20.41	11.41	13.87	0.69
	NF	7.02	55.86	14.67	22.45	0.00
	NF-s	37.50	29.39	6.53	25.02	1.55
PBS	**Ti**	0.00	53.93	20.76	25.32	0.00
	Ti-s	42.65	22.29	9.60	24.16	1.31
	NF	4.37	64.83	15.33	15.47	0.00
	NF-s	40.98	28.09	7.52	22.78	0.63

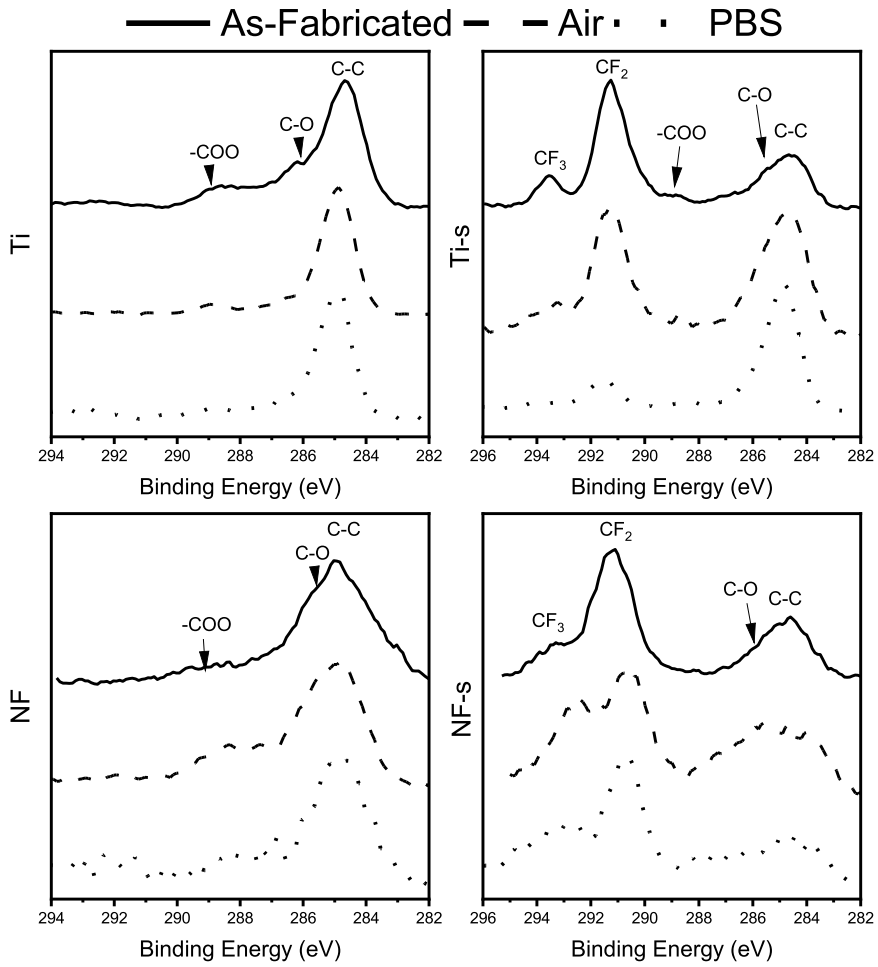

Figure 2.3.5: High resolution C1s XPS scans of as-fabricated surfaces and surfaces incubated in air and PBS for 4 weeks.

REFERENCES

[1] G. Wu, J. Wang, D.F. Thomas, A. Chen, Synthesis of F-Doped Flower-like TiO 2 Nanostructures with High Photoelectrochemical Activity, Lan. 24 (2008) 3503–3509. https://doi.org/10.1021/la703098g.

[2] V. Leszczak, K.C. Popat, Improved in Vitro Blood Compatibility of Polycaprolactone Nanowire Surfaces, Appl. Mater. Interfaces. 6 (2014) 15913–15924. https://doi.org/10.1021/am503508r.

[3] C.C. Mohan, K.P. Chennazhi, D. Menon, In vitro hemocompatibility and vascular endothelial cell functionality on titania nanostructures under static and dynamic conditions for improved coronary stenting applications, Acta Biomater. (2013). https://doi.org/10.1016/j.actbio.2013.08.023.

[4] M. Weber, H. Steinle, S. Golombek, L. Hann, C. Schlensak, H.P. Wendel, M. Avci-Adali, Blood-Contacting Biomaterials: In Vitro Evaluation of the Hemocompatibility, Front. Bioeng. Biotechnol. 6 (2018) 99. https://doi.org/10.3389/fbioe.2018.00099.

[5] R.M. Sabino, K. Kauk, L.Y.C. Madruga, M.J. Kipper, A.F. Martins, K.C. Popat, Enhanced hemocompatibility and antibacterial activity on titania nanotubes with tanfloc/heparin polyelectrolyte multilayers, J. Biomed. Mater. Res. - Part A. 108 (2020) 992–1005. https://doi.org/10.1002/jbm.a.36876.

[6] V. Leszczak, B.S. Smith, K.C. Popat, Hemocompatibility of polymeric nanostructured surfaces., J. Biomater. Sci. Polym. Ed. 24 (2013) 1529–48. https://doi.org/10.1080/09205063.2013.777228.

[7] M. Zhang, P. Wang, H. Sun, Z. Wang, Superhydrophobic Surface with Hierarchical Architecture and Bimetallic Composition for Enhanced Antibacterial Activity, Appl. Mater. Interfaces. 6 (2014) 22108–22115. https://doi.org/10.1021/am505490w.

[8] V.K. Manivasagam, K.C. Popat, In Vitro Investigation of Hemocompatibility of Hydrothermally Treated Titanium and Titanium Alloy Surfaces, ACS Omega. (2020) acsomega.0c00281. https://doi.org/10.1021/acsomega.0c00281.

[9] J. Vishnu, V. K Manivasagam, V. Gopal, C. Bartomeu Garcia, P. Hameed, G. Manivasagam, T.J. Webster, Hydrothermal treatment of etched titanium: A potential surface nano-modification technique for enhanced biocompatibility, Nanomedicine Nanotechnology, Biol. Med. 20 (2019) 102016. https://doi.org/10.1016/j.nano.2019.102016.

[10] S. Movafaghi, V. Leszczak, W. Wang, J.A. Sorkin, L.P. Dasi, K.C. Popat, A.K. Kota, Hemocompatibility of Superhemophobic Titania Surfaces, Adv. Healthc. Mater. (2016). https://doi.org/10.1002/adhm.201600717.

[11] A.T. Sidambe, Biocompatibility of advanced manufactured titanium implants-A review, Materials (Basel). 7 (2014) 8168–8188. https://doi.org/10.3390/ma7128168.

[12] P. Heinl, L. Müller, C. Körner, R.F. Singer, F.A. Müller, Cellular Ti-6Al-4V structures with interconnected macro porosity for bone implants fabricated by selective electron beam melting, Acta Biomater. 4 (2008) 1536–1544. https://doi.org/10.1016/j.actbio.2008.03.013.

[13] C. Yan, L. Hao, A. Hussein, P. Young, Ti-6Al-4V triply periodic minimal surface structures for bone implants fabricated via selective laser melting, J. Mech. Behav. Biomed. Mater. 51 (2015) 61–73. https://doi.org/10.1016/j.jmbbm.2015.06.024.

[14] J.W. Park, H.K. Kim, Y.J. Kim, J.H. Jang, H. Song, T. Hanawa, Osteoblast response and osseointegration of a Ti-6Al-4V alloy implant incorporating strontium, Acta Biomater. 6 (2010) 2843–2851. https://doi.org/10.1016/j.actbio.2010.01.017.

[15] J.M. Macák, H. Tsuchiya, P. Schmuki, High-aspect-ratio TiO2 nanotubes by anodization of titanium, Angew. Chemie - Int. Ed. 44 (2005) 2100–2102. https://doi.org/10.1002/anie.200462459.

[16] B. Arkles, Silane Coupling Agents Connecting Across Boundaries, 2014. http://www.kellychemical.com (accessed April 21, 2020).

[17] A.K. Kota, G. Kwon, A. Tuteja, The design and applications of superomniphobic surfaces, NPG Asia Mater. 6 (2014) e109–e109. https://doi.org/10.1038/am.2014.34.

[18] J. Drelich, E. Chibowski, D.D. Meng, K. Terpilowski, Hydrophilic and superhydrophilic surfaces and materials, Soft Matter. 7 (2011) 9804–9828. https://doi.org/10.1039/c1sm05849e.

[19] D. Zhang, G. Li, H. Wang, K.M. Chan, J.C. Yu, Biocompatible Anatase Single-Crystal Photocatalysts with Tunable Percentage of Reactive Facets, Cryst. Growth Des. 10 (2010) 1130–1137. https://doi.org/10.1021/cg900961k.

[20] R. Imani, V. Kralj-Iglič, A. Iglič, TiO2 nanostructures in biomedicine, in: Adv. Biomembr. Lipid Self-Assembly, Elsevier B.V., 2016: pp. 163–207. https://doi.org/10.1016/bs.abl.2016.05.002.

[21] J.A. Sorkin, S. Hughes, P. Soares, K.C. Popat, Titania nanotube arrays as interfaces for neural prostheses., Mater. Sci. Eng. C. Mater. Biol. Appl. 49 (2015) 735–745. https://doi.org/10.1016/j.msec.2015.01.077.

[22] M. Xu, G. Sun, C.-J. Kim, Infinite Lifetime of Underwater Superhydrophobic States, Phys. Rev. Lett. 113 (2014). https://doi.org/10.1103/PhysRevLett.113.136103.

[23] R.M. Sabino, K. Kauk, S. Movafaghi, A. Kota, K.C. Popat, Interaction of blood plasma proteins with superhemophobic titania nanotube surfaces, Nanomedicine Nanotechnology, Biol. Med. 21 (2019). https://doi.org/10.1016/j.nano.2019.102046.

CHAPTER 3

HEMOCOMPATIBILITY OF TITANIA NANOFLOWER SURFACES

3.1 Introduction

Thrombosis may occur on biomedical devices in contact with blood and cause life-threatening blood clots. Superhydrophobic materials offer a materials-based solution to thrombosis on these devices without the need for long-lasting systemic drug therapies. The amplified contact angle produced by superhydrophobic materials may significantly reduce the contact between blood components and a device's surface. Past research with superhydrophobic titania nanostructures indicated improved hemocompatibility by limiting platelet and leukocyte adhesion and activation [1,2]. The limited adhesion and activation of cells on surfaces is a result of limited blood-plasma protein adsorption. In this work, superhydrophobic titania nanoflowers were characterized by protein adsorption, cytotoxicity, adhesion and activation of platelets, adhesion of leukocytes, and whole blood clotting to determine the surface's hemocompatibility.

3.2 Materials and Methods

3.2.1 Surface sterilization and incubation in hemocompatibility studies

Different characterization techniques were used to evaluate the hemocompatibility and on surfaces. The surfaces were prepared the same way for all the characterization techniques except for the whole blood clotting study. Surfaces were sterilized under UV light for 30 mins and rinsed with sterile PBS 3 times. Sterilized surfaces in hemocompatibility studies were placed in a 48-well plate and incubated in 400 µL of 100µg/mL PBS protein solution or platelet rich plasma (PRP) for 2 hours at 37˚C and 5% CO_2 on a shaker plate set to 100 rpm. All solutions were aspirated after incubation and rinsed 3 times with PBS.

3.2.2 Protein adsorption onto surfaces

The adsorption of blood serum proteins, fibrinogen and albumin, on surfaces was characterized using XPS. After incubation in protein solution and rinsing with PBS, the surfaces were rinsed 2 times with DI water to remove any un-adsorbed proteins. Survey spectra collected from 0 to 1100 eV and resolution N1s scans from 395 to 410eV. Peak-fit analysis was done using Multipack and OriginLab software.

3.2.3 Isolation of platelet-rich plasma (PRP)

Whole human blood was extracted from healthy adult individuals using 10 mL Vacuum Tubes containing the anticoagulant ethylenediaminetetraacetic acid (EDTA). The procedure for blood drawing from healthy donors was approved by Colorado State University Institutional Review Board and performed by a trained phlebotomist at the Colorado State University Health Center. Following a protocol described elsewhere, the first tube was discarded as waste, accounting for locally activated platelets due to needle insertion [3]. To separate the PRP from the whole blood, the tubes were centrifuged at 150g for 15 mins. The PRP was then pooled into a single tube and used within 2 hrs.

3.2.4 Cytotoxicity of surfaces

The cytotoxicity of surfaces was characterized using a commercially available lactate dehydrogenase (LDH) assay. After incubation in PRP, 100 µL of surface-exposed PRP was removed and added to wells in a 96-well plate. Subsequently, 100 µL of LDH solution was added to each well and incubated 30 mins at room temperature. Finally, the mixed solution was read at 490 nm using a plate reader to determine the amount of LDH released by the cells.

3.2.5 Cell adhesion onto surfaces

Cell adhesion on surfaces was characterized using a Zeiss Axio Imager.A2 fluorescence microscope. After incubation in PRP and rinsing in PBS, the surfaces were incubated with a 2 μM calcein-AM PBS solution for 20 mins in a dark atmosphere to avoid light exposure. The stain solution was then aspirated, and the surfaces rinsed 2 times in PBS before fluorescence imaging. Cell adhesion area coverage was calculated using ImageJ software.

3.2.6 Identification of platelets and leukocytes on surfaces

Identification of platelets and leukocytes adhered on surfaces was characterized using fluorescence microscopy. Rhodamine-phalloidin was used to stain the cell cytoskeleton protein, actin, which will stain red in both platelets and leukocytes; while DAPI (4',6-diamidino-2-phenylindole) was used to stain the cell nuclei, which will only stain blue in leukocytes. After incubation in PRP and rinsing in PBS, surfaces were incubated in a fixative of 3.7% formaldehyde PBS solution for 15 mins and rinsed 3 times with PBS. Subsequently, the surfaces were incubated in a permeative of 1% Triton X in PBS solution for 3 mins and rinsed 2 more times with PBS. 400 μL of rhodamine-phalloidin in PBS (1:200 concentration) was added to each well and allowed to incubate for 20 mins. After 20 mins, 42 μL of DAPI was added to each well and incubated for 5 additional minutes. Finally, the solution was aspirated, and the surfaces were rinsed 2 times with PBS before being imaged under a fluorescence microscope. Cell adhesion area coverage and the number of cell nuclei were calculated using Image J software.

3.2.7 Platelet activation on surfaces

Platelet activation on surfaces was characterized using SEM imaging. After incubation in PRP and rinsing in PBS, surfaces were incubated for 45 mins in a primary fixative solution comprised of 3% glutaraldehyde, 0.1 M sodium cacodylate, and 0.1 M sucrose in DI water. The surfaces were then moved to a glass dish and incubated for 10 mins in a buffer solution of 0.1 M

sodium cacodylate, and 0.1 M sucrose in DI water. Finally, they were moved to a separate glass dish and dehydrated in solutions of 35, 50, 70, and 100 % Ethanol in DI water for 10 mins each. The surfaces were coated with 10 nm of gold and imaged using SEM at 5 kV. The platelets visualized using SEM were classified into three different categories based on their morphologies:

- Unactivated (U): Platelets were essentially circular with no dendrite extension to the surface.
- Partially activated (P): Platelets displayed a few, short dendrites attached to the surface.
- Fully activated (F): Platelets displayed significant dendrite formation and attachment to the surface.

3.2.8 Whole blood clotting on surfaces

Whole blood clotting on surfaces was evaluated using a plate reader. The surfaces were sterilized under UV light for 30 mins and rinsed with sterile PBS 3 times. Sterilized surfaces were placed in a 24-well plate and 10 µL of whole blood droplets were placed on the surface. The blood was allowed to clot for 15, 30, or 45 mins. After the specific time interval, 1 mL of DI water was added to wells. The plate was then placed on a shaker plate at 100 rpm for 1 minute and allowed to rest for 5 mins. 200 µL of the un-clotted blood and DI water solution was then transferred to a 96-well plate and read at 540 nm.

3.2.9 Statistical analysis

Surface characterizations with SEM were done using at least 3 different surfaces for each surface type at 5 different locations on the surface (n_{min}=15). All hemocompatibility characterizations mentioned were completed at least 3 times with PRP taken from 3 different individuals (n_{min}=9). However, the results shown in each study are only from one individual since there is a large amount of variability in platelet count among donors. Statistical one-way ANOVA and student t-tests were completed for all quantitative results. Results were considered

statistically significant with a p-value ≤0.05. Analysis was done using JMP and OriginLab software.

3.3 Results and Discussion

3.3.1 Cytotoxicity of different surfaces

Before a surface can be implemented in a biomedical device, it must be shown to be non-cytotoxic. In this study, a commercially available LDH assay was used to determine the cytotoxicity of all surfaces. LDH is an enzyme released when the plasma membranes of cells (in this study, platelets and leukocytes) are damaged [4]. The assay works by using LDH to catalyze several reactions that result in the formation of formazan, which can be read for absorbance in a plate reader and is proportional to LDH release. Results show all surfaces in comparison to a negative (-) and positive (+) control (**figure 3.3.1**). A negative control indicates a sterilized well plate where PRP was placed unaltered and a positive control indicates a sterilized well plate where PRP was lysed to observe maximum LDH release. All surfaces showed negligible cytotoxicity compared to the positive control, and no significant difference in cytotoxicity was found between the surfaces and negative control.

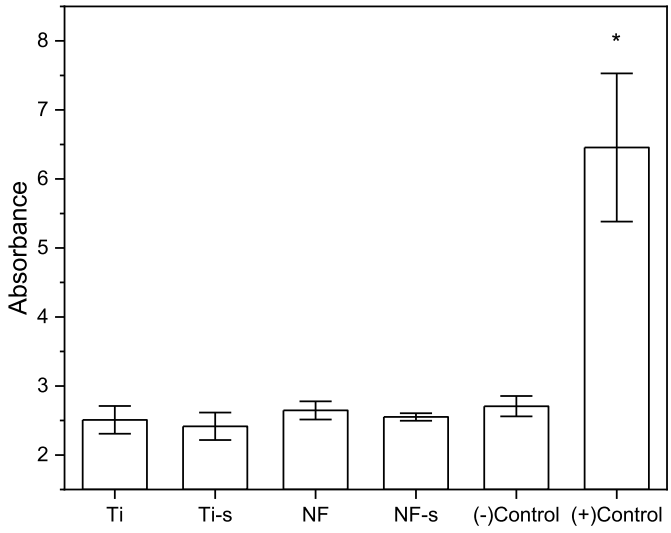

Figure 3.3.1: Cytotoxicity results from a commercially available LDH assay. All surfaces showed minimal cytotoxicity compared to the positive control (p≤0.05).

3.3.2 Protein adsorption on different surfaces

The very beginning stages of thrombosis on a surface involve the deposition and adsorption of blood-plasma proteins that form a foundation for inducing future platelet, leukocyte, and blood cell attachment [5]. The primary protein involved in thrombosis is fibrinogen. When it attaches to a surface, it is central to binding platelet integrin receptors which leads to platelet activation and aggregation [6]. In contrast, albumin, the most prominent blood-plasma protein, behaves passively and inhibits protein adhesion which can indirectly reduce platelet activation and adhesion [7]. Fibrinogen's shape is characterized as long and narrow while the shape of albumin is globular, which leads to easier unfolding and attachment on titania nano-textured surfaces [1]. Hence, it was expected that fibrinogen would adsorb more readily onto surfaces than albumin. In this study, surfaces were incubated in a fibrinogen or albumin solution. Protein adsorption was characterized using XPS scans by detecting the presence of nitrogen N1s peak (**figure 3.3.2**). The N1s peak is characteristic of protein adsorption because it is not present on any of the surfaces prior to protein adsorption [1]. As expected, the results indicate the highest percentage of elemental nitrogen was found on Ti for surfaces incubated in fibrinogen (**Table 3.3.1**). This was followed by NF, Ti-s, and NF-s. For surfaces incubated in albumin, Ti was also found to have the highest adsorption followed by Ti-s, NF, and NF-s. The results show reduced adsorption of both proteins on NF-s due to its superhydrophobic nature. The reduced adsorption of fibrinogen on NF-s suggests a reduction of subsequent platelet adhesion and activation.

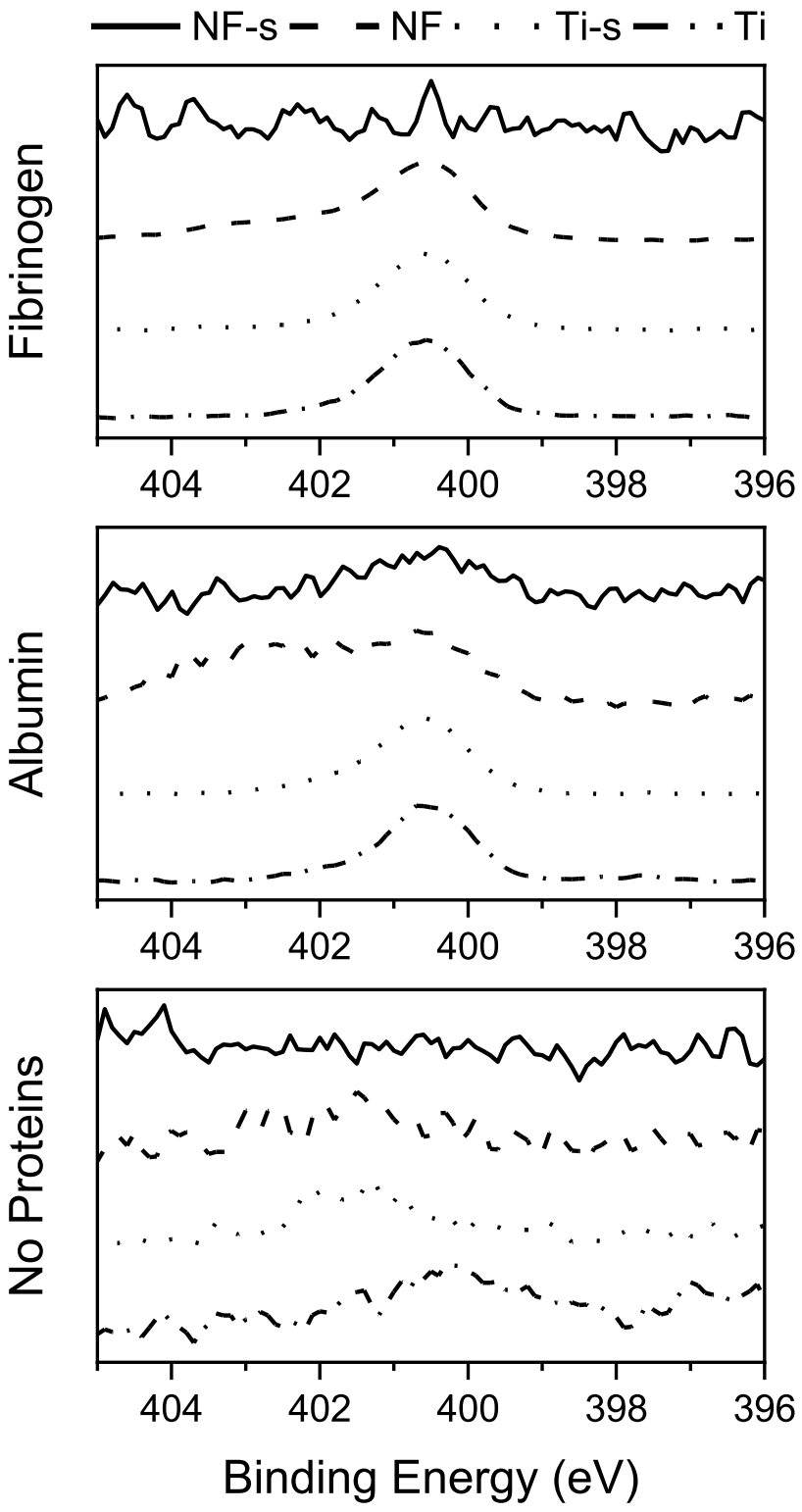

Figure 3.3.2: High resolution N1s XPS scans indicate the presence of protein on the surfaces.

Table 3.3.1: Elemental nitrogen percentage on different surfaces taken from XPS survey scans.

	Fibrinogen	Albumin
Ti	12.73%	5.50%
Ti-s	10.39%	4.7%
NF	11.29%	2.87%
NF-s	0.95%	0.72%

3.3.3 Cell adhesion on different surfaces

Following protein adsorption, platelets adhere and then activate on an artificial surface [5]. Activated platelets aid in modulating the activation of leukocytes in the blood stream, which leads to the formation of platelet-leukocyte aggregates [8]. Leukocytes can also promote platelet/leukocyte activation themselves and the blocking of coagulation inhibitors [9]. Therefore, a surface that prevents adhesion of platelets and leukocytes is ideal for reducing future activation and thrombosis. In this study, fluorescence microscopy was used to characterize platelet and leukocyte cell adhesion on surfaces after incubation in isolated PRP. The resulting images show platelets and leukocytes uniformly distributed on Ti, Ti-s, and NF (**figure 3.3.3A**). By contrast, NF-s showed cells sparsely adhered across the surface. Quantification of the images indicates no significant difference between Ti and NF cell adhesion (**figure 3.3.3B**). Ti-s showed a significant reduction when compared to both Ti and NF ($p \leq 0.05$) and NF-s had the least cell adhesion compared to all surfaces ($p \leq 0.05$).

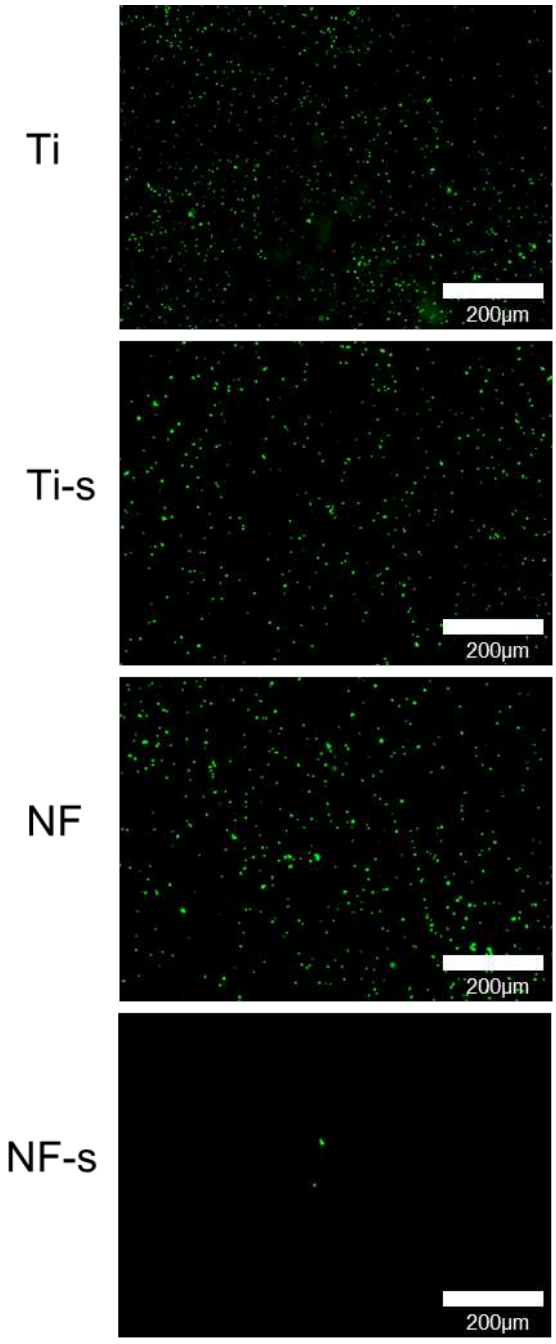

(A)

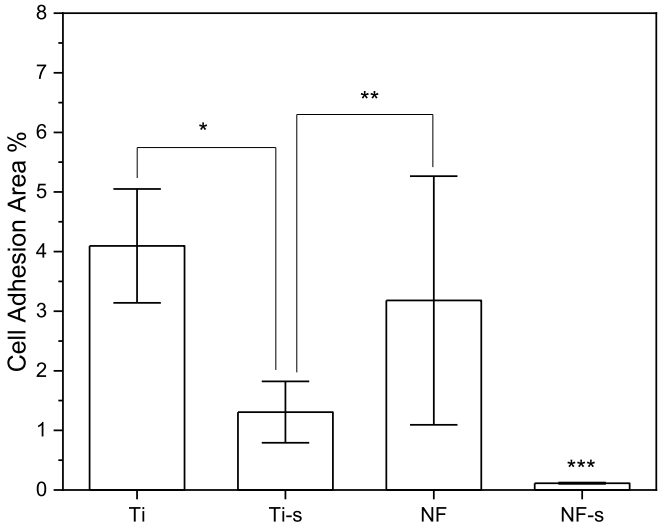

(B)

Figure 3.3.3: (A) Representative fluorescence microscopy images of calcein-AM-stained cells on different surfaces. **(B)** Cell surface adhesion area as a percentage on different surfaces (calcein-AM stain). NF-s showed significantly lower cell adhesion ($p \leq 0.05$).

Calcein-AM stained cells do not differentiate between platelet and leukocyte adhesion. For this reason, another staining was performed, which utilized rhodamine-phalloidin and DAPI stains to distinguish the two cell types. Rhodamine-phalloidin stains all cell cytoskeletons red while DAPI solely stains the nuclei of cells blue. Since platelets do not have a nucleus, only leukocytes are stained by DAPI. The resulting rhodamine-phalloidin images show platelets and leukocytes uniformly distributed on Ti, Ti-s, and NF (**figure 3.3.4A**). By contrast, NF-s showed cells sparsely adhered across the surface. Quantification of these images indicates no significant difference between Ti, Ti-s, and NF cell adhesion (**figure 3.3.4B**). NF-s showed a significant reduction in adhesion when compared to all other surfaces ($p \leq 0.05$), which agrees with calcein-AM adhesion results. The DAPI images show leukocytes present on Ti, Ti-s, and NF (**figure 3.3.4A**) with fewer leukocytes visible on NF-s. Quantification of these images indicates a significant reduction between Ti and all other surfaces ($p \leq 0.05$) (**figure 3.3.4C**). NF-s was shown to have a significantly lower number of leukocytes than all other surfaces as well ($p \leq 0.05$).

As expected, the results from all cell adhesion characterizations (**figure 3.3.3-4**) indicated more adhesion on Ti, Ti-s, and NF in comparison to NF-s. The change of surface nanotexture between Ti and NF only lowered adhesion in the case of leukocytes, but not platelets. The effect of lowering surface energy between Ti and Ti-s appeared to reduce overall adhesion to a larger degree. However, the combination of the nanotexture and lowered surface energy on NF-s significantly reduced cell adhesion due to the lowered interaction between PRP and the surface, suggesting NF-s may reduce the body's inflammatory response.

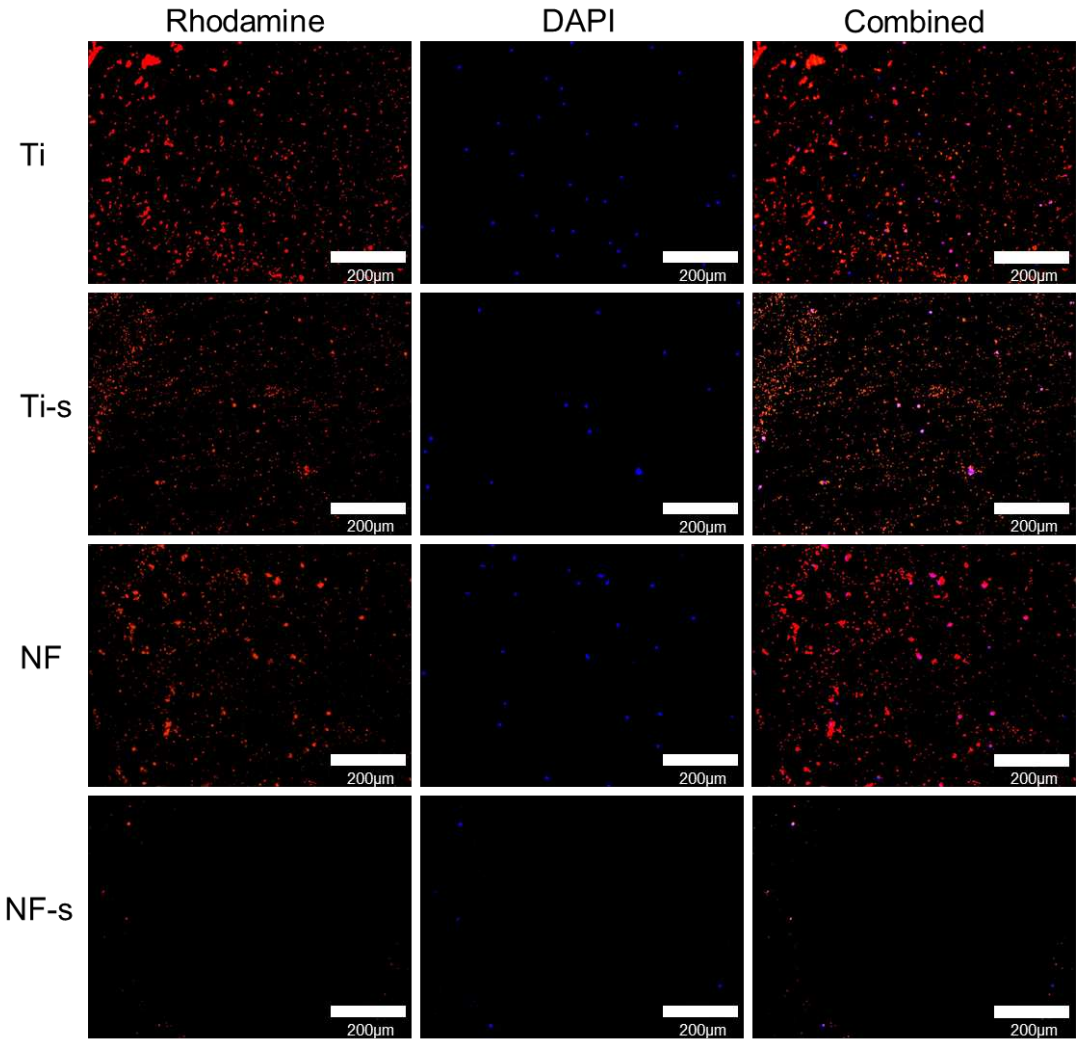

(A)

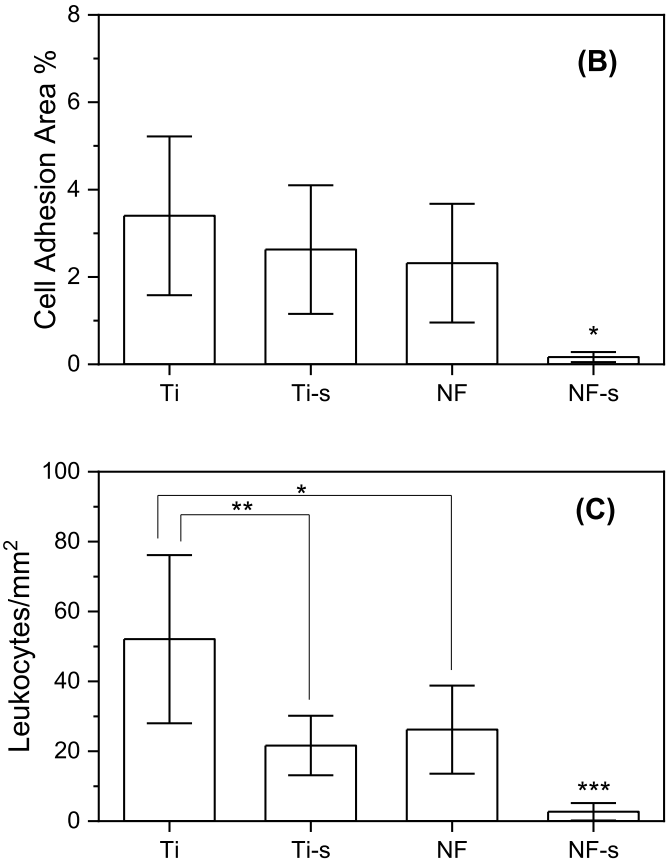

Figure 3.3.4: (A) Representative fluorescence microscopy images of rhodamine-phalloidin and DAPI stained cells on different surfaces. **(B)** Cell surface adhesion area as a percentage on different surfaces (rhodamine-phalloidin stain) and **(C)** Leukocytes per mm^2 (DAPI stain). NF-s showed significantly lower cell and leukocyte adhesion ($p \leq 0.05$).

3.3.4 Platelet activation on different surfaces

When platelets are activated they change morphologies by forming dendrites that attach to the surface and other platelets [10]. This activation is a prerequisite to blood-clotting and full thrombosis [5]. Platelet activation was characterized through SEM imagery. The results show large networks of platelets adhered and activated on Ti, Ti-s, and NF (**figure 3.3.5A**). NF-s did not show these networks and very few platelets were found on the surface. Before quantification, the platelets adhered to the surface were categorized as unactivated, partially activated, or fully activated based on criteria outlined in section **2.9**. No statistical difference was observed in the number of unactivated, partially activated, or fully activated platelets between Ti and Ti-s (**figure**

3.3.5B). Furthermore, neither unactivated or partially activated platelets were found on NF or NF-s. There was a statistically significant increase in fully activated platelets on NF compared to all surfaces ($p \leq 0.05$), which may be due to the high surface roughness allowing for more surface area for platelets to attach and form dendrites. Finally, NF-s showed the least amount of fully activated platelets compared to all other surfaces ($p \leq 0.05$), which was expected considering its reduced protein adsorption and platelet adhesion.

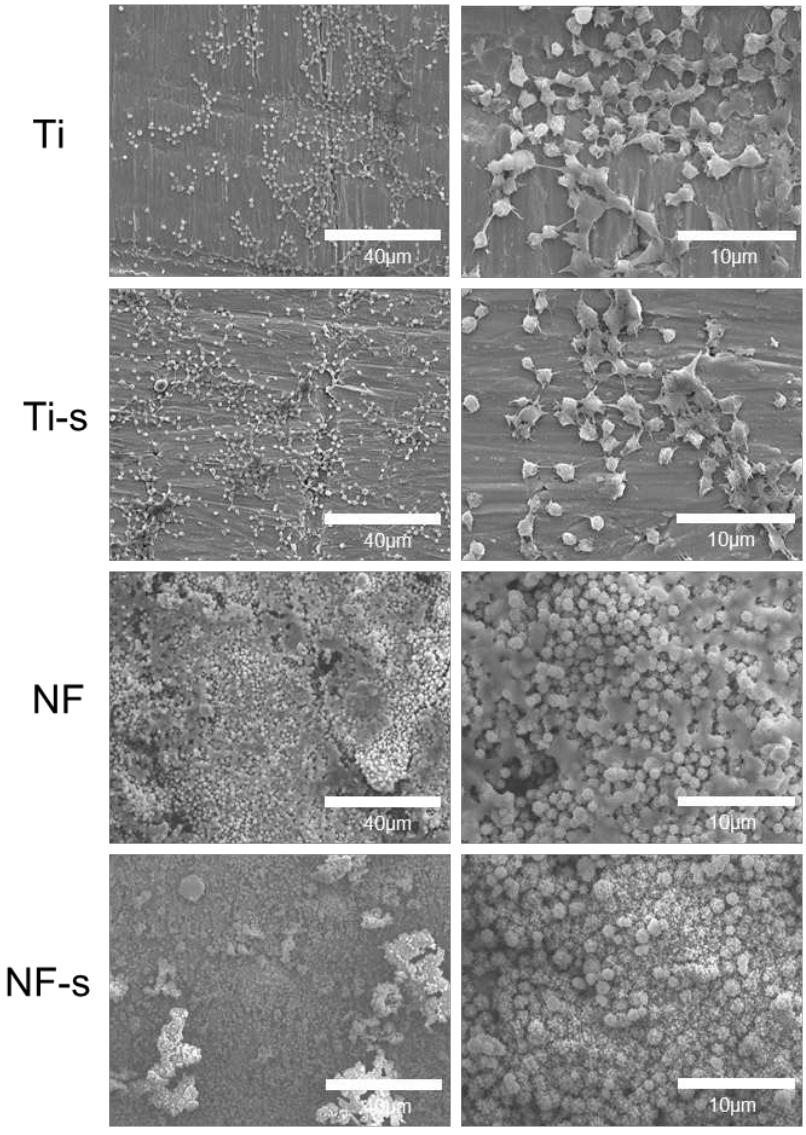

(A)

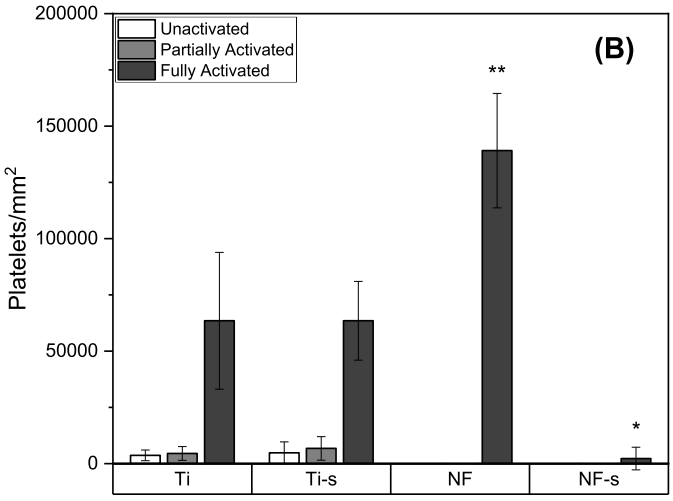

Figure 3.3.5: (A) Representative SEM images of cell activation on various surfaces. **(B)** Platelet count on different surfaces. NF-s was shown to have the lowest number of fully activated platelets ($p \leq 0.05$).

3.3.5 Whole blood clotting on different surfaces

Reduction of whole blood clotting is important for long-term hemocompatibility. Within the coagulation cascade, formation of a fibrin matrix follows platelet activation, which traps red blood cells and forms a clot [3,11]. Clot formation can result in a failure of the device and injury to the patient, such as stroke. In this study, whole blood clotting was characterized by measuring free hemoglobin with an absorption plate reader after 15, 30, and 45-minute clotting periods. Blood was allowed to clot on surfaces for the given amount of time, after which DI water was added to the surface to dissolve and lyse whole blood cells that were not trapped in the fibrin matrix, releasing hemoglobin into the solution [12]. Hence, higher absorbance values indicated more free hemoglobin in solution and thus less blood clotting on the surface (**figure 3.3.6**). Both Ti and NF showed considerable blood clotting. After 30 mins on Ti, there was significantly more clotting on the surface. No significant changes were seen for Ti-s, NF, or NF-s in clotting over 45 mins. After 45 mins, NF-s indicated the lowest amount of clotting of any surface ($p \leq 0.05$). This was expected based on results for NF-s from the aforementioned hemocompatibility characterizations and suggests NF-s may improve hemocompatibility of a blood-contacting biomedical device.

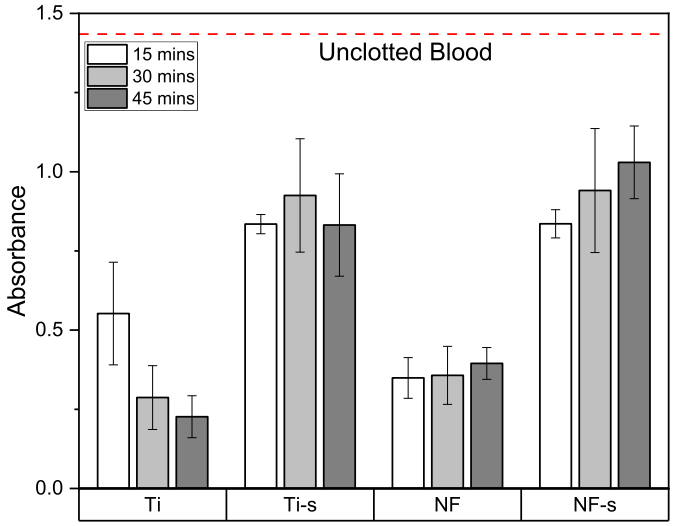

Figure 3.3.6: Whole blood clotting indicated by free hemoglobin absorbance measured after 15, 30, and 45 mins. Note: statistics are discussed in results and discussion.

REFERENCES

[1] K. Bartlet, S. Movafaghi, A. Kota, K.C. Popat, Superhemophobic titania nanotube array surfaces for blood contacting medical devices, R. Soc. Chem. Adv. 7 (2017) 35466–35476. https://doi.org/10.1039/c7ra03373g.

[2] S. Movafaghi, V. Leszczak, W. Wang, J.A. Sorkin, L.P. Dasi, K.C. Popat, A.K. Kota, Hemocompatibility of Superhemophobic Titania Surfaces, Adv. Healthc. Mater. (2016). https://doi.org/10.1002/adhm.201600717.

[3] V. Leszczak, B.S. Smith, K.C. Popat, Hemocompatibility of polymeric nanostructured surfaces., J. Biomater. Sci. Polym. Ed. 24 (2013) 1529–48. https://doi.org/10.1080/09205063.2013.777228.

[4] Thermo Fisher Scientific, CyQUANT™ LDH Cytotoxicity Assay, 2019. https://www.thermofisher.com/order/catalog/product/C20301#/C20301 (accessed April 29, 2020).

[5] I.H. Jaffer, J.C. Fredenburgh, J. Hirsh, J.I. Weitz, Medical device-induced thrombosis: what causes it and how can we prevent it?, J. Thromb. Haemost. 13 (2015) S72–S81. https://doi.org/10.1111/jth.12961.

[6] S.L. Goodman, S.L. Cooper, R.M. Albrecht, Integrin receptors and platelet adhesion to synthetic surfaces, J. Biomed. Mater. Res. 27 (1993) 683–695. https://doi.org/10.1002/jbm.820270516.

[7] L.C. Xu, J.W. Bauer, C.A. Siedlecki, Proteins, platelets, and blood coagulation at biomaterial interfaces, Colloids Surfaces B Biointerfaces. 124 (2014) 49–68. https://doi.org/10.1016/j.colsurfb.2014.09.040.

[8] L.L. Swystun, P.C. Liaw, The role of leukocytes in thrombosis, Blood. 128 (2016) 753–762. https://doi.org/10.1182/blood-2016-05-718114.

[9] M.B. Gorbet, M. V. Sefton, Biomaterial-associated thrombosis: Roles of coagulation factors, complement, platelets and leukocytes, Biomaterials. 25 (2004) 5681–5703. https://doi.org/10.1016/j.biomaterials.2004.01.023.

[10] Q. Huang, Y. Yang, R. Hu, C. Lin, L. Sun, E.A. Vogler, Reduced platelet adhesion and improved corrosion resistance of superhydrophobic TiO2-nanotube-coated 316L stainless steel, Colloids Surfaces B Biointerfaces. 125 (2015) 134–141. https://doi.org/10.1016/j.colsurfb.2014.11.028.

[11] R.M. Sabino, K. Kauk, S. Movafaghi, A. Kota, K.C. Popat, Interaction of blood plasma proteins with superhemophobic titania nanotube surfaces, Nanomedicine Nanotechnology, Biol. Med. 21 (2019). https://doi.org/10.1016/j.nano.2019.102046.

[12] R. Sabino, K. Popat, Evaluating Whole Blood Clotting in vitro on Biomaterial Surfaces, BIO-PROTOCOL. 10 (2020). https://doi.org/10.21769/bioprotoc.3505.

CHAPTER 4

BACTERIAL ADHESION ON TITANIA NANOFLOWERS

4.1 Introduction

Bacterial infection occurs on many blood-contacting biomedical devices. Infection begins through the adhesion of bacteria onto the surface and often results in the formation of microcolonies known as biofilms. Biofilm infections are incredibly difficult to treat with classic antibiotic treatment. Therefore, researchers are looking towards material-based solutions that stop bacterial adhesion, and thus, biofilms before they begin. Superhydrophobic materials significantly reduce the contact between aqueous media and surface features, making it difficult for bacteria to adhere. In this work, superhydrophobic titania nanoflowers were characterized for their bacterial adhesion and biofilm formation of both Gram-negative and Gram-positive bacteria after 6 and 24 hr incubation periods.

4.2 Materials and Methods

4.2.1 Surface sterilization and incubation in bacterial studies

Different characterization techniques were used to evaluate bacterial adhesion on surfaces. Surfaces were sterilized under UV light for 30 mins and rinsed with sterile PBS 3 times. Sterilized surfaces in bacterial studies were placed in a 48-well plate and incubated in 500 µL of bacterial solution for either 6 or 24 hours at 37˚C. All solutions were aspirated after incubation and rinsed 3 times with PBS.

4.2.2 Preparation of bacteria cultures

Bacterial strains of *Escherichia coli* (E. *coli*) and *Staphylococcus aureus* (*S. aureus*) were used to characterize the behavior of Gram-negative and Gram-positive bacteria on surfaces, respectively. Bacterial colonies were introduced into 5 mL of trypsin soy broth (TSB) used as a

bacterial growth media and vortexed for 10 seconds to properly mix the bacteria within the media before incubation for 6 hours at 37˚C. After incubation, 200 µL of solution was added to a 96-well plate. Three dilutions of the solution were made to create different bacterial concentrations, and the plate was subsequently read at a wavelength of 562 nm in a plate reader to determine optical density. A dilution was made until the solution obtained an average optical density of 0.52, indicating a concentration of 10^9 bacterial cells/mL TSB solution. Once this was achieved, the solution was further diluted with TSB to obtain a 10^6 bacterial cells/mL TSB solution.

4.2.3 Bacteria adhesion on surfaces

Bacteria adhesion on surfaces was characterized using fluorescence microscopy. After incubation and rinsing in PBS surfaces were moved to a new 48-well plate. A fluorescence stain was made using a commercially available live/dead bacteria staining assay with SYTO® 9 and propidium iodide. In a dark environment, 500 µL of stain solution was added to each well and incubated for 20 mins at room temperature. The stain solution was removed, and the surfaces rinsed with PBS before being fixed in a 3.7% formaldehyde PBS solution for 15 mins. Finally, the fixative was aspirated, and the surfaces rinsed in PBS before imaging under a Zeiss fluorescence microscope. Bacteria adhesion area coverage was calculated using Image J software.

4.2.4 Bacteria morphology on surfaces

Bacteria morphology on surfaces was characterized using SEM imaging. After incubation in PRP and rinsing in PBS, surfaces were incubated for 45 mins in a primary fixative solution comprised of 3% glutaraldehyde, 0.1 M sodium cacodylate, and 0.1 M sucrose in DI water. The surfaces were then moved to a glass dish and incubated for 10 mins in a buffer solution of 0.1 M sodium cacodylate, and 0.1 M sucrose in DI water. Finally, the substrates were moved to a separate glass dish and dehydrated in solutions of 35, 50, 70, and 100 % Ethanol in DI water for 10 mins each. The surfaces were coated with 10 nm of gold and imaged using SEM at 5 kV.

4.2.5 Statistical analysis

Surface characterizations with SEM were confirmed on at least 2 different samples of each surface. The fluorescence stains were completed at least 3 times with 3 different surfaces for each bacteria and time period (n_{min}=9). SEM fixing was repeated 3 times with 3 different surfaces for each bacteria and time period (n_{min}=9). Statistical one-way ANOVA and student t-tests were completed for all quantitative results. Results were considered statistically significant with a p-value ≤0.05. Analysis was done using JMP and OriginLab software.

4.3 Results and Discussion

4.3.1 Bacterial adhesion and biofilm formation

Bacterial infection presents another issue for blood-contacting biomedical devices. Bloodstream infections are most common in patients with catheters and can lead to sepsis or even death [1]. Bacterial colonies grown on implant surfaces often lead to biofilm formation, which can protect the bacteria from antibiotics [2]. Infectious bacteria can be divided into two different types: Gram-positive and Gram-negative. These two bacterial types differ in many ways. One prominent difference is in cell-wall thickness and composition, where Gram-positive bacteria generally have thick peptidoglycan layers on top of a phospholipid cytoplasmic membrane, and Gram-negative bacteria have thin peptidoglycan layers in between two inner and outer cytoplasmic membrane [3]. In this study, *Staphylococcus aureus* and *Escherichia coli* were chosen to characterize the behavior of Gram-positive and Gram-negative bacterial on surfaces, respectively. *S. aureus* is a Gram-positive bacterial strain commonly associated with infections on medical devices and can even be found on human skin [2]. *E. coli*, while not often associated with medical device infections, is similar in structure to *P. aeruginosa*, a more prevalent infectious bacterial strain [4], and thus served as a model for the behavior of Gram-negative bacteria. Since

both bacterial types may require different treatments [5], it is essential to characterize their respective behaviors on a biomedical device surface.

Fluorescence microscopy was used to characterize adhesion of bacteria on all surfaces. A commercially available live/dead bacteria assay containing two stains (Syto-9 and propidium iodide) was used to differentiate between bacteria that were alive after incubation and those that were dead. Syto-9 stains both living and dead bacteria, while propidium iodide only stains dead bacteria. Syto-9 appears green in fluorescence images and propidium iodide appears red. Images taken of surfaces incubated in both bacterial types generally showed more living bacteria than dead bacteria. Images of surfaces incubated in *S. aureus* indicate bacterial adhesion onto Ti, Ti-s, and NF after 6 hrs and reduced adhesion on NF-s (**figure 4.3.1A**). After 24 hrs, increased bacterial adhesion is observed on all surfaces compared to 6 hrs, however, there is lower overall adhesion on NF-s. The quantified results indicate that both live and dead bacterial adhesion increased after 24 hrs for Ti and NF ($p \leq 0.05$) (**figure 4.3.1B,C**). Live and dead bacterial adhesion did not significantly change after 24 hrs for both Ti-s and NF-s. Live bacterial adhesion after 24 hrs was shown to be the least on NF-s compared to all other surfaces ($p \leq 0.05$). Dead bacterial adhesion after 24 hrs was lowest on Ti-s and NF-s and no significant difference was found between the two.

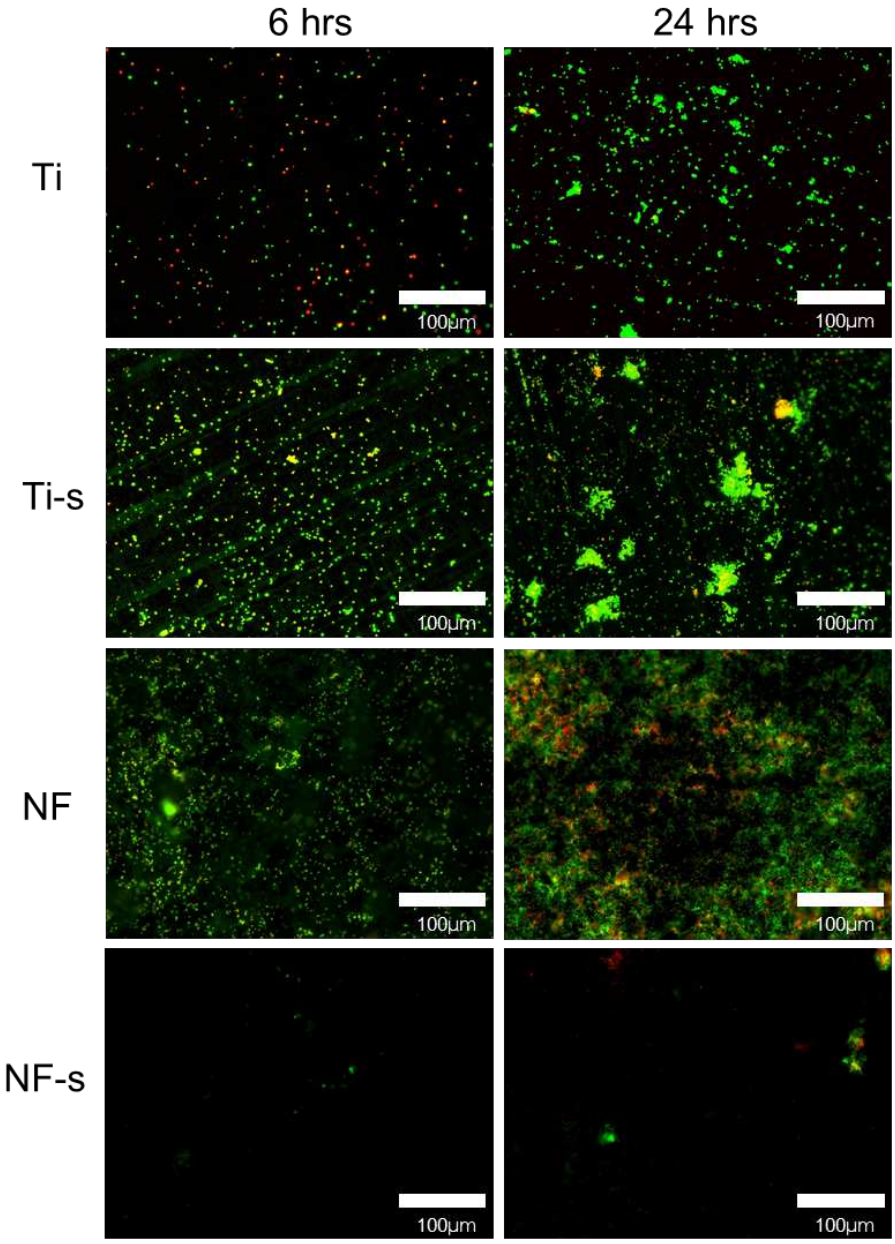

(A)

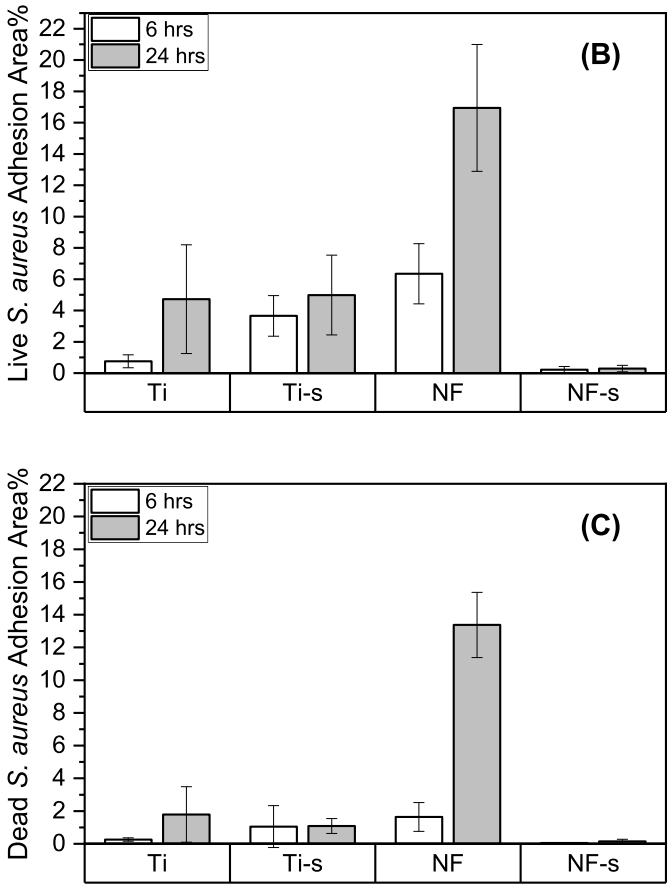

Figure 4.3.1: (A) Representative fluorescence images of *S. aureus* on different surfaces. Bacterial cell adhesion area percentage for live **(B)** and dead **(C)** *S. aureus* after 6 and 24 hrs. Note: statistics discussed in results and discussion.

Images of surfaces incubated in *E. coli* indicate bacterial adhesion onto Ti, Ti-s, and NF after 6 hrs and reduced adhesion on NF-s (**figure 4.3.2A**). After 24 hrs, increased bacterial adhesion is observed on all surfaces relative to 6 hrs, however, adhesion is still comparatively less on NF-s. The quantified results indicate that live bacterial adhesion increased after 24 hrs on Ti-s and NF ($p \leq 0.05$) (**figure 4.3.2B, C**). Live bacterial adhesion did not significantly change after 24 hrs for both Ti and NF-s and was shown to be the least on NF-s compared to all surfaces ($p \leq 0.05$). No significant difference was found on Ti, Ti-s, or NF for dead bacterial adhesion after 24 hrs compared to 6 hrs. Both Ti and NF-s after 24 hrs were found to have the lowest dead bacterial adhesion compared to all other surfaces ($p \leq 0.05$).

In general, dead bacterial adhesion was comparable between Gram-positive and Gram-negative bacteria. The bactericidal effects of the surfaces can be interpreted as minimal since the number of dead bacteria was either much less than or equal to the number of live bacteria on every surface. Overall, the findings suggest reduced liquid-surface interaction on superhydrophobic NF-s inhibited the growth and formation of colonies for both Gram-positive and Gram-negative bacteria.

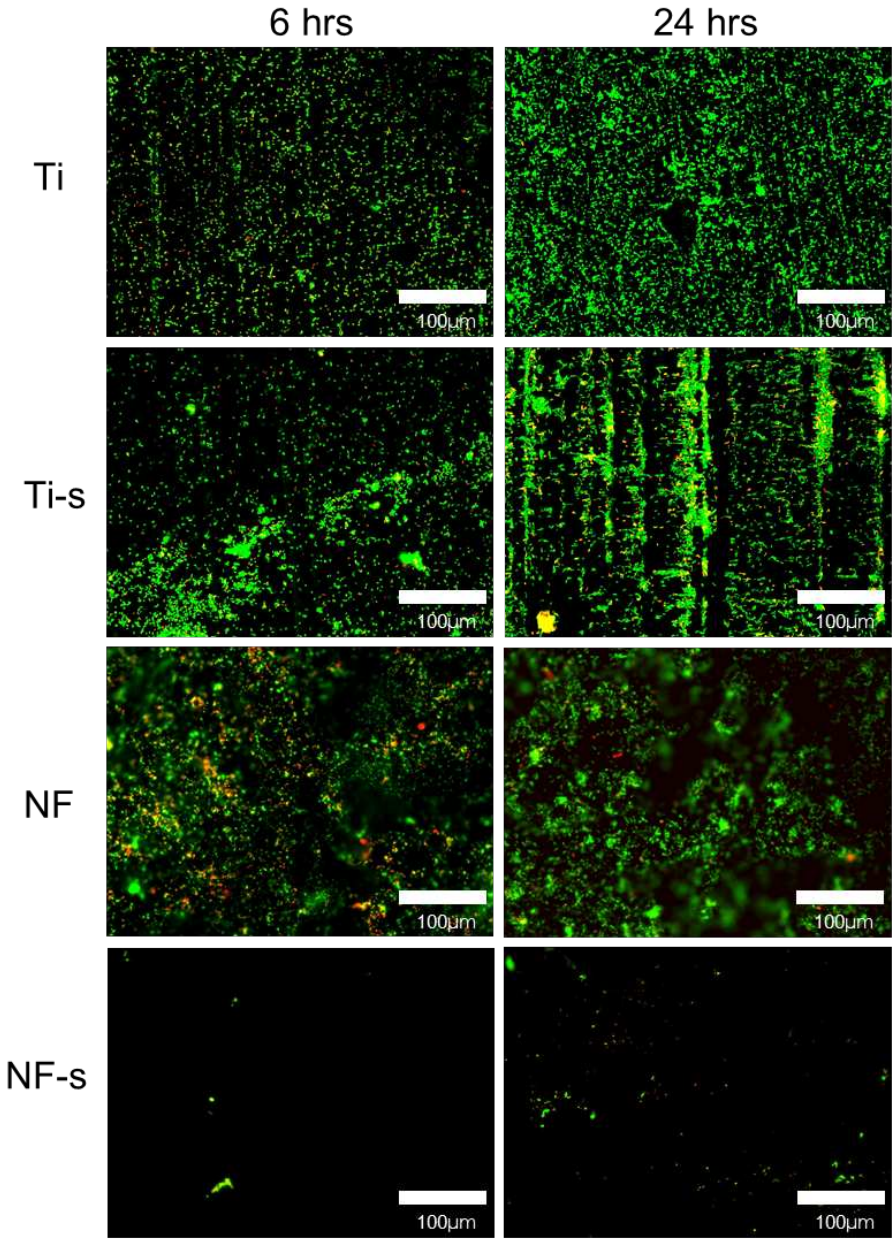

(A)

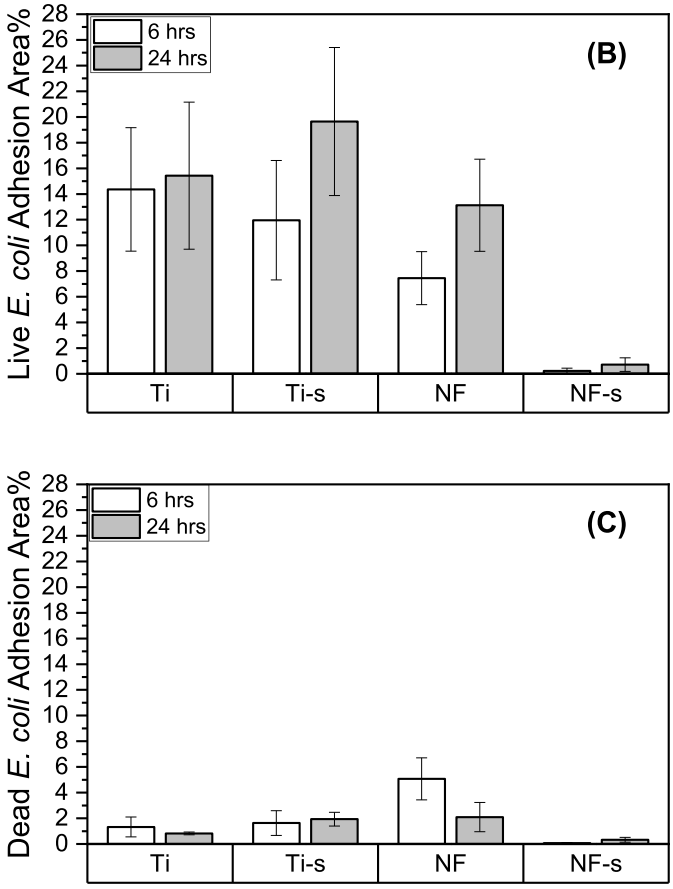

Figure 4.3.2: (A) Representative fluorescence images of *E. coli* on different surfaces. Bacterial cell adhesion area percentage for live **(B)** and dead **(C)** *E. coli* after 6 and 24 hrs. Note: statistics discussed in results and discussion.

4.3.2 Bacterial morphology

Following bacterial adhesion, biofilms form and create a network that provides protection bacterial cells. Certain genes that code for multidrug resistance can more readily be shared between bacterial plasmids within the film, increasing antibiotic resistance [1,6]. Since there is often not an effective solution to destroying a biofilm, the best solution is to prevent its formation [1,7], which may be achieved by altering the biomaterial's surface. In this work, biofilm formation was characterized using SEM images. The results for *S. aureus* showed more adhesion after 24 hrs compared to 6 hrs on all surfaces (**figure 4.3.3A**). This was consistent with the results found from fluorescence images found previously. After 6 hrs, colonies of bacteria began to form on Ti,

Ti-s, and NF. After 24 hrs, larger colonies are formed on all surfaces and biofilm formation appears to begin on Ti and NF. After 6 hrs no bacteria were visible on the NF-s surface. After 24 hrs, small colonies began to form, but were scattered sparsely and only seen on damaged parts of the surface. The results for *E. coli* showed more adhesion after 24 hrs compared to 6 hrs on Ti, Ti-s and NF (**figure 4.3.3B**). This was consistent with the results found from fluorescence images. After 6 hrs, colonies of bacteria began to form on Ti, Ti-s, and NF. After 24 hrs, larger colonies are formed on these surfaces and biofilm formation appears to begin on Ti-s. After 6 hrs and 24 hrs, no bacteria were visible on the NF-s surface. Overall, the results suggest that the superhydrophobic NF-s surface helped to inhibit adhesion and biofilm formation of both Gram-positive and Gram-negative bacteria.

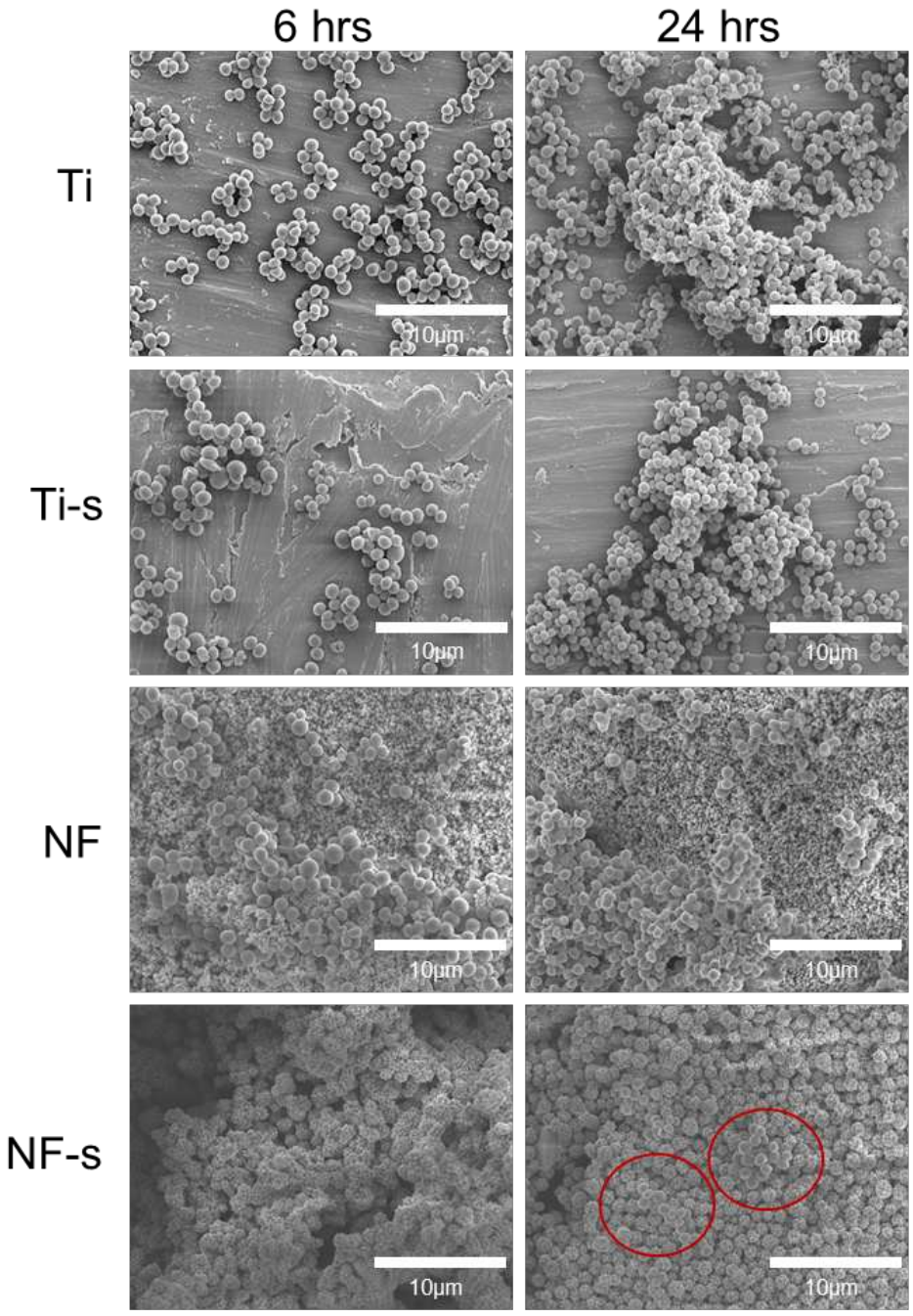

(A)

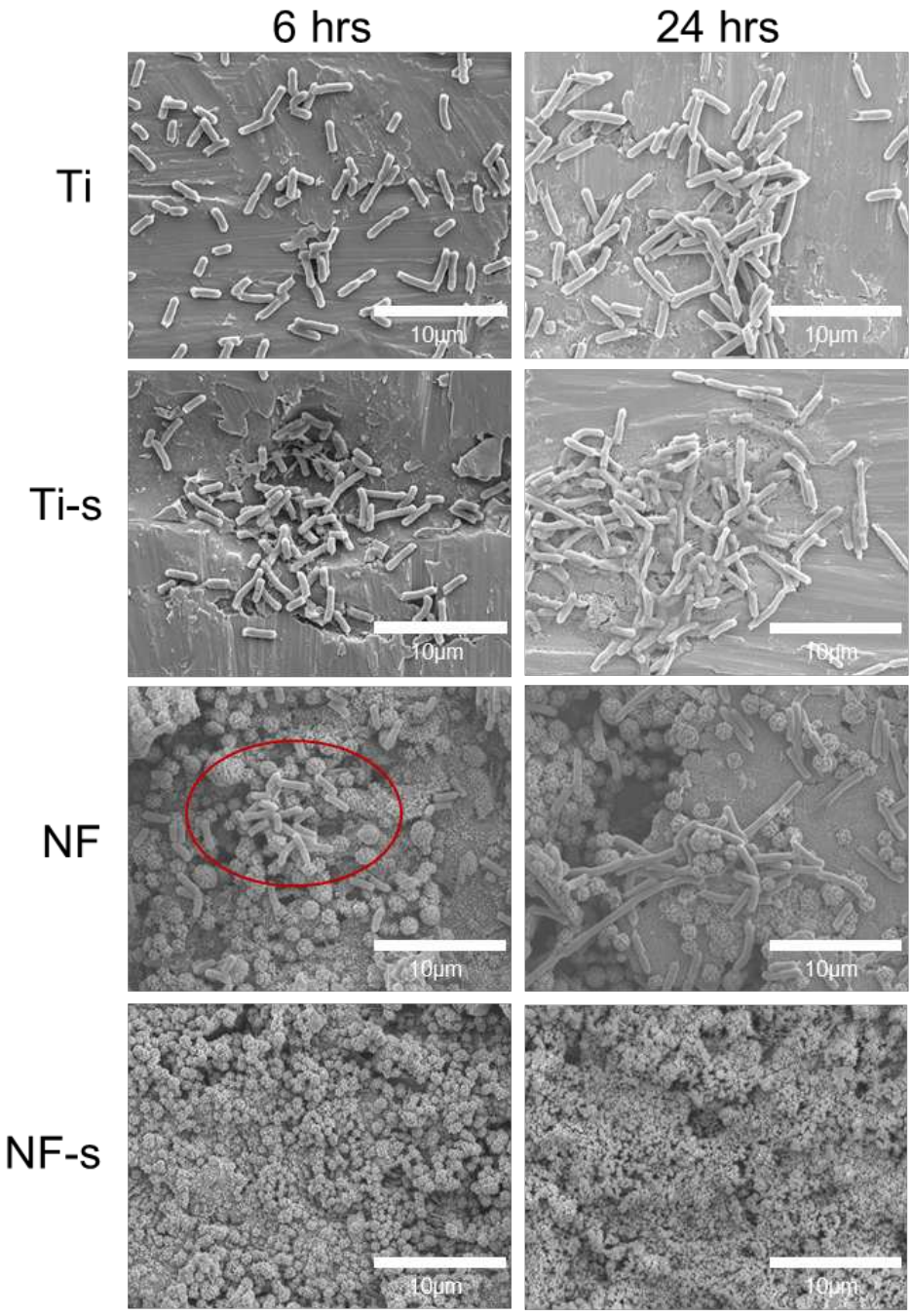

(B)

Figure 4.3.3: Representative SEM images of *S. aureus* **(A)** and *E. coli* **(B)** on different surfaces.

REFERENCES

[1] I. Francolini, G. Donelli, Prevention and control of biofilm-based medical-device-related infections, FEMS Immunol. Med. Microbiol. 59 (2010) 227–238. https://doi.org/10.1111/j.1574-695X.2010.00665.x.

[2] K. Bartlet, S. Movafaghi, L.P. Dasi, A.K. Kota, K.C. Popat, Antibacterial activity on superhydrophobic titania nanotube arrays, Colloids Surfaces B Biointerfaces. 166 (2018) 179–186. https://doi.org/10.1016/j.colsurfb.2018.03.019.

[3] A.T. Poortinga, R. Bos, W. Norde, H.J. Busscher, Electric double layer interactions in bacterial adhesion to surfaces, Surf. Sci. Rep. 47 (2002) 1–32.

[4] L.C. Xu, M.E. Meyerhoff, C.A. Siedlecki, Blood coagulation response and bacterial adhesion to biomimetic polyurethane biomaterials prepared with surface texturing and nitric oxide release, Acta Biomater. 84 (2019) 77–87. https://doi.org/10.1016/j.actbio.2018.11.035.

[5] R.O. Darouiche, Device-Associated Infections: A Macroproblem that Starts with Microadherence, Clin. Infect. Dis. 33 (2001) 1567–1572. https://doi.org/10.1086/323130.

[6] R.M. Donlan, Biofilms: Microbial life on surfaces, Emerg. Infect. Dis. 8 (2002) 881–890. https://doi.org/10.3201/eid0809.020063.

[7] M. Habash, G. Reid, Microbial biofilms: Their development and significance for medical device-related infections, J. Clin. Pharmacol. 39 (1999) 887–898. https://doi.org/10.1177/00912709922008506.

CHAPTER 5

CONCLUSIONS AND FUTURE WORK

5.1 Conclusions

Blood-contacting medical devices used today can be susceptible to thrombosis and bacterial infection when implanted into the body. Thrombosis begins rapidly when blood-plasma proteins first encounter and adsorb onto a device surface. This triggers platelet adhesion and activation, immune response, and eventually blood clotting. Devices can also become colonized by bacteria, which may lead to persistent biofilm infections. These complications can cause device failure or be life-threatening. Current solutions to thrombosis and bacterial infection often involve long-term drug therapies or device replacement. Thus, researchers are searching for effective materials-based solutions to these problems. Superhydrophobic materials have impressive antiadhesive properties, making them promising candidates for the prevention of fouling by blood and bacteria on device surfaces. However, very few studies have investigated their potential in blood-contacting medical devices. In this study, superhydrophobic titania nanoflowers were fabricated and characterized for their material properties, hemocompatibility, and bacterial adhesion.

Titania nanoflower surfaces were fabricated and evaluated for their surface properties before undergoing hemocompatibility and bacterial adhesion characterizations. Fabrication was accomplished with a simple hydrothermal synthesis procedure performed with Ti-6Al-4V substrates, an aqueous HF solution, and heat. Superhydrophobic titania nanoflowers were subsequently manufactured via vapor-phase deposition of a fluorine-based silane compound. Analysis of surface morphology revealed insignificant changes between silanized and unsilanized titania nanoflowers. Surface chemistry analysis revealed changes in fluorine and carbon functional groups on superhydrophobic titania nanoflowers compared to untreated surfaces,

indicating successful silanization. Surface crystallography analysis indicated no significant differences in TiO_2 material properties after hydrothermal synthesis or silanization. Superhydrophobicity was confirmed by contact angles >150° and roll-off angles <10° after silanization. Contact angles >150° and key carbon-fluorine functional groups remained after 4 weeks of incubation in PBS, indicating surface stability.

The hemocompatibility titania nanoflower surfaces was investigated following fabrication and material characterization. Short term cytotoxicity was evaluated with an LDH assay and the surfaces were found to be non-toxic. Adsorption of blood-plasma proteins, albumin and fibrinogen, was evaluated via XPS analysis. Superhydrophobic titania nanoflowers were found to have less adsorption of both proteins compared to the untextured and untreated surface. Reduced protein adsorption resulted in lower adhesion and activation of platelets, and lower leukocyte adhesion, indicating a decreased immune response. This culminated in reduced blood clotting compared to all other surfaces.

Bacterial adhesion on titania nanoflowers was characterized with Gram-positive (*S. aureus*) and Gram-negative bacteria (*E. coli*). Fluorescence imaging results indicate very little adhesion of either *S. aureus* or *E. coli* on superhydrophobic titania nanoflowers after 24 hrs, and significantly less adhesion compared to unmodified and untextured surfaces. The number of live bacteria was either similar or greater than the number of dead bacteria on every surface examined, indicating the surfaces were not bactericidal. SEM imaging results indicate no significant biofilm formation on superhydrophobic titania nanoflowers after 24 hrs for either bacteria types. Biofilm formation did appear on unmodified and untextured surfaces.

In summary, superhydrophobic titania nanoflower surfaces fabricated on Ti-6Al-4V substrates were found to be stable after 4 weeks of incubation in PBS. In addition, the surface indicated reduced adhesion of blood components and bacteria. These results suggest

superhydrophobic titania nanoflowers can provide a stable medical device surface that prevents thrombosis and biofilm infection.

5.2 Future Work

In future studies, more specific protein characterizations should be performed on superhydrophobic titania nanoflowers. Protein deposition is a crucial step for thrombosis and biofilm formation. Proteins like factor XII are central to thrombosis on medical devices, so behavior of this protein on these surfaces should be investigated. Furthermore, an ELISA protein assay could be performed after adsorption to determine a more accurate blood-plasma protein profile. Knowledge of the specific proteins on the surface may help determine better engineering solutions. Future blood compatibility and bacterial characterizations should focus on the longevity of surface effects. Surfaces should be exposed to plasma and bacteria for longer than 2 and 24 hours, respectively, to determine if adhesion remains limited after long-term exposure. In addition, implanted surfaces are exposed to the dynamic flow conditions of the biological environment, thus, surfaces should be characterized under flow conditions within the lab. Finally, a significant problem facing superhydrophobic materials is their tendency to lose their effect over longer periods of time. The superhydrophobic surfaces in this study remained stable after incubation in PBS for at least 4 weeks under static conditions. However, future studies must examine the ability for these surfaces to remain stable much longer. Titania nanostructured surfaces are generally fragile and easily damaged. If the surface is damaged, the surface will lose antiadhesive properties and prove ineffective. Therefore, future research must find methods to make these surfaces more durable.